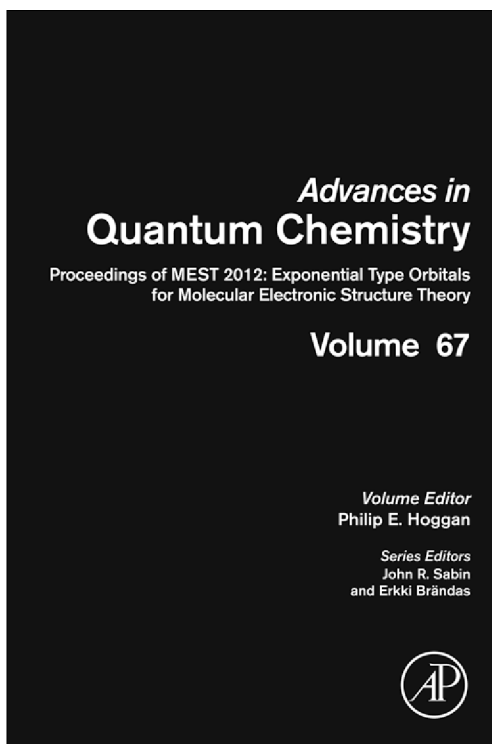


**Provided for non-commercial research and educational use only.
Not for reproduction, distribution or commercial use.**

This chapter was originally published in the book *Proceedings of MEST 2012: Exponential Type Orbitals for Molecular Electronic Structure Theory*. The copy attached is provided by Elsevier for the author's benefit and for the benefit of the author's institution, for non-commercial research, and educational use. This includes without limitation use in instruction at your institution, distribution to specific colleagues, and providing a copy to your institution's administrator.



All other uses, reproduction and distribution, including without limitation commercial reprints, selling or licensing copies or access, or posting on open internet sites, your personal or institution's website or repository, are prohibited. For exceptions, permission may be sought for such use through Elsevier's permissions site at:

<http://www.elsevier.com/locate/permissionusematerial>

From G. Gasaneo et al., Three-Body Coulomb Problems with Generalized Sturmian Functions. In: Philip E. Hoggan, editor, *Proceedings of MEST 2012: Exponential Type Orbitals for Molecular Electronic Structure Theory*. Vol 67, Chennai: Academic Press, 2013, p. 153-216.

ISBN: 978-0-12-411544-6

© Copyright 2013 Elsevier Inc.

Academic Press.



Three-Body Coulomb Problems with Generalized Sturmian Functions

G. Gasaneo^a, L.U. Ancarani^b, D.M. Mitnik^c, J.M. Randazzo^d,
A.L. Frapiccini^a and F.D. Colavecchia^d

^aDepartamento de Física, Universidad Nacional del Sur and IFISUR-CONICET, Bahía Blanca, Argentina

^bThéorie, Modélisation, Simulation, SRSMC, UMR CNRS 7565, Université de Lorraine, 57078 Metz, France

^cInstituto de Astronomía y Física del Espacio (IAFE), CONICET and Departamento de Física, FCEyN, Universidad de Buenos Aires, Argentina

^dDivisión Colisiones Atómicas, Centro Atómico Bariloche and CONICET, Río Negro, Argentina

Contents

1. Introduction	154
2. Generalized Sturmian functions	157
2.1 Definitions	157
2.2 Bound states	160
2.3 Scattering states	163
3. Three-body problems: bound states	167
3.1 Systems with general masses	168
3.2 Two-electron atoms	170
3.3 Finite mass exotic and molecular systems	175
3.4 Confined atoms	178
4. Three-body problems: scattering states	182
4.1 Introduction	182
4.2 Asymptotic behaviors	183
4.3 Driven equation for three-body scattering problems	185
4.4 Solving the driven equation with GSF (spherical coordinates)	189
4.5 Solving the driven equation with GSF (hyperspherical coordinates)	190
5. Three-body scattering states: applications	195
5.1 Introduction	195
5.2 Three-body <i>S</i> -wave model problem	196
5.3 <i>S</i> -wave model of (<i>e</i> , 2 <i>e</i>) processes on hydrogen	201
5.4 <i>S</i> -wave model of (<i>e</i> , 3 <i>e</i>) processes on helium	204
6. Summary and perspectives	208
Acknowledgments	210
References	210

Abstract

The study of structure and collision processes of three- and four-body problems has seen an extraordinary progress in the last decades. This progress has been in part associated to the incredible fast growth of the computer capabilities. However, the tools used to solve structure problems are different from those corresponding to the treatment of collision processes. In this review, we provide the theoretical framework and a selection of results for both structure as well as collision problems using only one technique that we have developed in the last few years, based on the use of Generalized Sturmian functions. We present results obtained in structure studies of isolated and confined two-electron atoms, and exotic and molecular systems. The same technique is applied to the study of various benchmark problems for the single ionization of hydrogen and the double ionization of helium by electron impact. In this way, we demonstrate that the Generalized Sturmian method can be successfully applied to the treatment of both types of problems.



1. INTRODUCTION

A wide variety of phenomena in atomic, molecular physics, or chemistry depend on the understanding of the three-body problem.¹ Many atomic and molecular processes in an extended range of energies present simultaneous excitation and ionization, double or multiple ionization of some of the electrons in the system. These processes cannot be treated with the standard *ab initio* methods designed to study structure, since emitted electrons are spread all over space. It is also difficult to deal with them using the methods designed specifically for atomic collision, since there, in general, the bound electrons are treated in approximate ways. Moreover, there are not many methods allowing the accurate and precise description of outgoing electrons and at the same time, providing on equal footing the correct initial bound state of a collision.

The study of atomic and molecular systems as presented in the literature can be separated into two branches, one devoted to the study of bound states and another focused on collision processes. For the bound state treatment of atomic and molecular systems, the use of spectral methods is a standard tool. The very well-established configuration interaction (*CI*) method rests on the use of the sum of basis functions to represent the wave function of the system.¹ The “configurations” are generally defined as the sum of products of basis functions associated with the description of the dynamics of two-particle interactions. For example, each of these functions is the solution of the electron–nucleus problem in the case of atoms, while

the nucleus–nucleus interactions are considered for molecules. Approaches like VASP² or Gaussian³ use basis functions very localized in configuration space to properly represent the dynamics of the electrons and the nuclei. These methods have proven to be very useful and robust, however, this does not necessarily result in efficiency. On the other hand, a well-known disadvantage of these methods is that they are unable to deal at all with the dynamics of a process involving the fragmentation of the system.

Quite recently, the idea of optimizing these existing methods for atomic and molecular structure calculations has taken a different line based on the replacement of Gaussian or Slater basis functions by Coulomb Sturmian functions (CSF),^{4–6} with a focus on bound-type states only. A fantastic advantage has been observed when CSF were applied, e.g., to the structure calculation of many-electron atoms. It was found that all the basis functions scale with a length parameter. This property allows reduction of the calculations of all the matrix elements to basically two types of integrals that can be evaluated only once for all the electrons of the system.⁵ From the collisional point of view, other difficulties arise.⁷ First, the wave function of an ejected particle is completely delocalized. Second, outgoing particles should have the correct asymptotic behavior, which implies considering large values of the emitted particle coordinates and, therefore, the whole problem has to be solved over very large numerical domains.⁸ Various techniques have been implemented to enforce those conditions or to circumvent them. Methods like the J-matrix^{9–11} and the convergent-close-coupling (CCC),¹² among others, impose the asymptotic conditions at high values of one coordinate but they do not necessarily represent the correct behavior in the region where all the emitted particles are far from each other; such domain is the most important, for example, when studying double ionization processes. A different methodology is implemented in the exterior complex scaling (ECS) approach.¹³ As often pointed out in the literature, this method avoids imposing the asymptotic condition because it sets an outgoing flux on the coordinates associated with the emitted (ionized) particles. Even if it is not yet totally clear how this happens,¹⁴ it has been confirmed with many numerical results that the correct three-body outgoing behavior is conferred on the wave function when this methodology is applied. All these approaches work very efficiently on the treatment of collision processes involving just a very few particles, leading to accurate solutions to, for example, the ionization of hydrogen by electron impact.¹⁵ The remarkable growth of computational capabilities has made possible the implementation of those recipes. However, computational limitations

do not allow, for the moment, their extension for more than two interacting electrons. For example, full time-independent calculations of a simple four-body problem, such as the double ionization of Helium by electron impact, are not yet available. The main limitation is, of course, the size of the equation systems to be solved.

It is important to point out that the CCC approach, for example, does not consider all the electrons on the same footing (one of the emitted electrons is treated differently from the others) bringing in some problems in the approach.¹⁶ On the other hand, the ECS treats the emitted electrons in the same way, rotating the coordinates to the complex plane for each electron and ending up in the continuum part of the spectra. The description of those electrons is done using spectral methods but with basis functions which, in most of the implementations, are purely numerical with no, or little, trace of the physics of the considered problem.

The synthesis of the aforementioned issues together with the aim of numerical basis optimization directed us to the Generalized Sturmian Functions (GSF) approach. Following the leading ideas of Avery¹⁷⁻¹⁹ and Aquilanti,²⁰⁻²³ on one side, and Rawitscher²⁴⁻²⁸ and Macek,²⁹⁻³⁴ on the other, starting nearly a decade ago³⁵ the present authors developed the approach thereafter.³⁶⁻⁴³ The GSF approach makes use of a combination of the best features of the precedent methods. On one hand, it treats the dynamics of the system's electrons on equal footing as each of them is represented by GSF. On the other hand, the asymptotic behavior of each particle is taken into account by the basis allowing matching of the expansion region to the reaction region, where all the dynamics takes place. For electrons, for example, some may be in the continuum while others occupy bound states: within the GSF method, they will be represented by basis functions that have proper outgoing or bound-type behavior, respectively. It has been already numerically demonstrated that the use of GSF basis with outgoing components allows the enforcement of three-body type outgoing behavior in a similar way as the ECS method does. Generally speaking, a distinctive feature of the GSF method is that it employs basis functions possessing physical properties similar to those corresponding to the system under study. Moreover, the use of GSF greatly increases the convergence rate of various physical quantities when dealing with bound states and reduces the computational resources required for describing scattering processes. It is the purpose of this work to review some of the aspects of the Generalized Sturmian function method that we developed.

This paper is organized as follows: In [Section 2](#) all the relevant information referred to the GSF for two-body problems is presented, as well as the theory corresponding to their application to bound and scattering problems involving only two-particles. Several relevant aspects of the method are introduced there, starting with the Sturm–Liouville equation for a general radial interaction, the boundary conditions, and the definition of the auxiliary and generating potentials of the GSF basis. A comparison with CSF is also presented. The remaining sections are devoted to the three-body problem. In [Section 3](#), the use of GSF to study three body Coulomb problems for particles of arbitrary masses is presented, focusing on the calculation of atomic and molecular structure. Calculations for a wide variety of systems are discussed, ranging from the negative Hydrogen ion and the largely studied Helium atom to more exotic muonic systems. Ground and excited states including the double excited states of Helium are considered. Also, very accurate energy values are presented for a Helium atom confined inside a model cage representing a fullerene molecule, or in an impenetrable box. In [Section 4](#), the GSF theory for three-body continuum states is described, both in spherical and in hyperspherical coordinates. The three-body asymptotic behavior for scattering problems is discussed, and the driven equations for two typical ionization processes are presented, illustrating the possible benefits of both systems of coordinates. In [Section 5](#), several examples of simple collision systems are developed, centering the attention on the properties of the wave function, the convergence of the method, and the extraction of cross-sections from the asymptotic flux. Finally, in [Section 6](#) the important features of the GSF method are summarized and some perspectives are outlined.

Atomic units are used through this paper, unless otherwise noted.



2. GENERALIZED STURMIAN FUNCTIONS

2.1 Definitions

The Generalized Sturmian functions to be studied and applied are all associated with the two-body problems described by the time-independent Schrödinger equation

$$\left[-\frac{1}{2\mu}\nabla^2 + \mathcal{U}(r) - E \right] \mathcal{S}(\mathbf{r}) = -\beta \mathcal{V}(r)\mathcal{S}(\mathbf{r}). \quad (1)$$

We are assuming here that $\mathcal{U}(r)$ and $\mathcal{V}(r)$ are spherically symmetric potentials. [Equation \(1\)](#) has three main parameters in addition to the reduced mass

μ , they are: the energy E , the magnitude of $\mathcal{U}(r)$, and the magnitude β of the potential $\mathcal{V}(r)$. The idea behind the Generalized Sturmian functions is to consider the energy E and the magnitude of $\mathcal{U}(r)$ as externally fixed parameters and β the eigenvalue of the problem. Given the fact that we will be dealing with spherically symmetric potentials, we can propose the separation on radial and angular variables $\mathcal{S}(\mathbf{r}) = S_{nl}(r) Y_{lm}(\theta, \phi)/r$. With this definition, the radial part of Eq. (1) transforms into

$$\left[-\frac{1}{2\mu} \frac{d^2}{dr^2} + \frac{l(l+1)}{2\mu r^2} + \mathcal{U}(r) - E \right] S_{nl}(r) = -\beta_{nl} \mathcal{V}(r) S_{nl}(r). \quad (2)$$

We name $\mathcal{U}(r)$ the *auxiliary* potential (e.g., Coulomb), and $\mathcal{V}(r)$ the *generating* potential defined in general to be of short-range i.e. vanishing in an outer region $r > R_S$. To transform the Schrödinger equation (2) into a Sturm–Liouville problem two boundary conditions are required. Throughout this paper, we seek solutions having a regular boundary condition at the origin

$$S_{nl}(r = 0) = 0. \quad (3)$$

If the auxiliary potential $\mathcal{U}(r)$ is a Coulomb potential, then, the Kato cusp condition can also be imposed through an appropriate choice of the potentials \mathcal{U} and \mathcal{V} , as discussed in. Ref. 42

In the outer region, where the second boundary condition is imposed, the generating potential vanishes. The radial Sturmian equation (2) reduces to

$$\left[-\frac{1}{2\mu} \frac{d^2}{dr^2} + \frac{l(l+1)}{2\mu r^2} + \mathcal{U}(r) - E \right] S_{nl}(r) = 0 \quad \text{for } r > R_S, \quad (4)$$

the solutions of which represent a particle of energy E moving under the influence of a potential $\mathcal{U}(r)$, and will have a unique asymptotic behavior, that is, independent of the eigenvalue β_{nl} .

Equation (2) together with the boundary conditions (3) and (4) define a Sturm–Liouville problem. Therefore, their solutions form a complete basis set with closure

$$\sum_n S_{nl}(r') \mathcal{V}(r) S_{nl}(r) = \delta(r - r'), \quad (5)$$

and obey a potential-weighted orthogonality relation:

$$\int_0^\infty S_{n'l}(r) \mathcal{V}(r) S_{nl}(r) dr = 0 \quad \text{for } n' \neq n. \quad (6)$$

Two important issues related to this orthogonality relation are worth of notice. First, due to the fact that the generating potential $\mathcal{V}(r)$ is of short-range, the integration (6) can be performed numerically in a finite spatial region for any value of the energy E , without any additional requirement over the $S_{nl}(r)$ functions. The second point to note is that the integral is defined without taking the complex conjugate of the function $S_{n'l}(r)$. With this particular choice of the scalar product, the overlaps between the functions:

$$\mathcal{O}_{n'n} = \int_0^\infty S_{n'l}(r) S_{nl}(r) dr \quad (7)$$

converge for any energy and potential (this was discussed in detail in Ref. 44). It is interesting to note that since the generating potential is of short-range, the boundary condition at large values of r can be imposed at any r value greater than R_S . This allows numerical construction of the functions in an efficient way. All the functions differ asymptotically from one another by a normalization factor.

Let us now illustrate that the $S_{nl}(r)$ functions have the same asymptotic behavior with different examples, beginning with the case of negative energies $E < 0$. For a short-range auxiliary potential $\mathcal{U}(r)$ (i.e., $\mathcal{U}(r)$ also vanishing in the outer region) the asymptotic solutions of (4) behave like

$$\lim_{r \rightarrow \infty} S_{nl} \propto e^{-\kappa r}, \quad (8)$$

where $\kappa = \sqrt{-2\mu E}$. Since E is a fixed parameter, all the basis functions have the same asymptotic behavior.

In the case of a Coulombic auxiliary potential $\mathcal{U}(r) = z_1 z_2 / r$ with z_1 positive and z_2 negative, the solutions of (2) have an asymptotic behavior consisting of an exponentially decaying factor $\exp(-\kappa r)$ modified by a logarithmic factor

$$\lim_{r \rightarrow \infty} S_{nl} \propto e^{-\kappa r - \frac{z_1 z_2 \mu}{\kappa} \ln(2\kappa r)}, \quad (9)$$

which is, again, the same for all basis elements.

When dealing with positive energies the expressions given by Eqs. (8) and (9) transform into

$$\lim_{r \rightarrow \infty} S_{nl} \propto e^{ikr}, \quad (10)$$

and

$$\lim_{r \rightarrow \infty} S_{nl} \propto e^{ikr - i \frac{z_1 z_2 \mu}{k} \ln(2kr)}, \quad (11)$$

respectively. These are the asymptotic solutions of Eq. (4) corresponding, respectively, to a short-range and a Coulomb-type auxiliary potential. Similar expressions for incoming waves can be also used.

At this point we would like to emphasize the difference between our Generalized Sturmian functions with the Coulombic auxiliary potential, and the widely used Coulomb Sturmian functions. The CSF are solutions of

$$\left[-\frac{1}{2\mu} \frac{d^2}{dr^2} + \frac{l(l+1)}{2\mu r^2} - E \right] S_{nl}^C(r) = \beta_{nl} \frac{1}{r} S_{nl}^C(r), \quad (12)$$

i.e., the same Eq. (2) with $\mathcal{U}(r) = 0$ and $\mathcal{V}(r) = -1/r$. The discretized character of the solutions imposes $\beta_{nl} = n\kappa$. In this case, the asymptotic behavior of the CSF is

$$\lim_{r \rightarrow \infty} S_{nl}^C \propto e^{-\kappa r + n \ln(2\kappa r)} = (2\kappa r)^n e^{-\kappa r}, \quad (13)$$

which changes from one CSF element to another, due to the presence of the power n . For positive energies, the asymptotic condition reads

$$\lim_{r \rightarrow \infty} S_{nl}^C \propto e^{ikr + \frac{Z_n \mu}{k} \ln(2kr)}, \quad (14)$$

where $Z_n = \beta_n = in\sqrt{2\mu E}$. All the functions oscillate with the same wave-number k (determined externally by the fixed energy) but each of them has a different logarithmic phase, depending on the eigenvalue.

2.2 Bound states

In this section, we briefly review the methodology for two-body bound states. For a given interaction potential $V(r)$, the aim is to solve the Schrödinger equation

$$\left[-\frac{1}{2\mu} \frac{d^2}{dr^2} + \frac{l(l+1)}{2\mu r^2} + V(r) - E \right] \Psi(r) = 0, \quad (15)$$

where, for bound states, the energy E is negative. The solution $\Psi_B(r)$ may be expanded as

$$\Psi_B(r) = \sum_n a_n S_{nl}(r). \quad (16)$$

Upon replacement in (15), and using (2) with energy E_s , we have

$$\sum_n a_n [V(r) - \mathcal{U}(r) - \beta_{nl} \mathcal{V}(r) - E + E_s] S_{nl}(r) = 0. \quad (17)$$

We may choose the auxiliary potential $\mathcal{U}(r)$ to be the interaction $V(r)$, so that the first two terms in Eq. (17) cancel each other. Projecting with basis functions $S_{n'l}(r)$ from the left, integrating over the coordinate, using the orthogonality relation (6) and the overlap matrix (7), we get

$$\sum_n [-\beta_{nl} \mathcal{V}'_{n'n} \delta'_{n'n} - (E - E_s) \mathcal{O}'_{n'n}] a_n = 0, \quad (18)$$

which can be easily solved by standard matrix methods.⁴⁰

2.2.1 Numerical implementation

Details of the numerical aspects involved in the generation of the Sturmian basis set are published in Ref. 43 and will not be repeated here. We will just mention that we use primarily a finite-differences scheme to solve Eq. (2). The boundary condition is imposed within this scheme, treating in a special way the last elements of the Hamiltonian matrix. The eigenvalues are initially calculated by using a complex-orthogonal transformation based on the theory explained by Luk and Qiao.⁴⁵ In previous work,^{38,39} we performed a further relaxation of a random vector multiplied by the Hamiltonian matrix, until it converges to the desired eigenvalue. In that procedure, the corresponding eigenvectors were also obtained. We also developed another very fast iterative algorithm that allows us to obtain very accurate eigenvalues. For any eigenvalue, the corresponding eigenvector is computed by using a predictor–corrector method. The procedure includes a numerical (outwards) integration from the origin to a particular matching point and another integration (inwards) from the asymptotic region to the

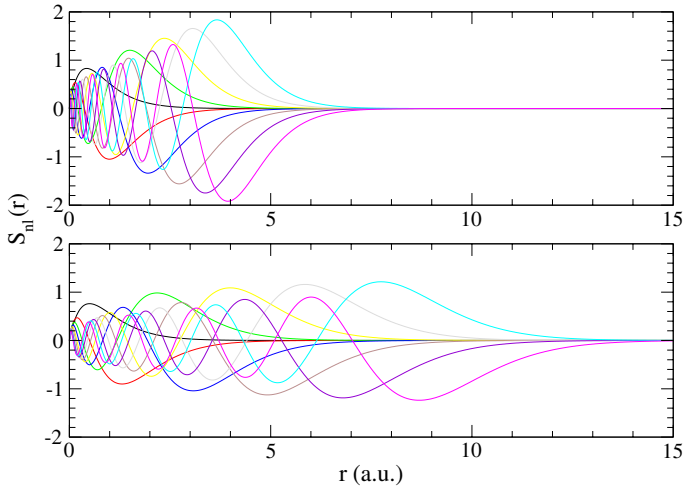


Figure 7.1 Up: First Generalized Sturmian functions S_{n0} for an auxiliary potential $\mathcal{U}(r) = 0$, a generating potential $\mathcal{V}(r) = e^{-0.375r}/r$, and an energy $E = -2.0$ a.u. Down: Coulomb Sturmian functions, for the same energy. For color version of this figure, the reader is referred to the online version of this chapter.

matching point. At this particular matching point the logarithmic derivatives are calculated for both solutions, and iterations are performed until the difference between both values becomes negligible.

For completeness, we should mention that we have also developed other implementations for GSF basis set generation. For example, in Ref. 41 we used a square integrable (L^2) basis set expansion with Laguerre-type basis functions⁴⁶ and B-spline functions.⁴⁷

2.2.2 Example

As an illustration, consider the case in which $E = -2.0$ a.u. and $l = 0$. Figure 7.1 displays (in the upper curves) the first 10 GSF corresponding to the case of a Coulomb auxiliary potential

$$\mathcal{U}(r) = -\frac{Z}{r}, \tag{19}$$

where $Z = 0$, and a Yukawa generating potential

$$\mathcal{V}(r) = -\frac{e^{-a_s r}}{r}, \tag{20}$$

with $a_s = 0.375$. For comparison the Coulomb Sturmian functions for the same energy are plotted in the lower part of the figure. Clearly, the CSF are

spread over a wide range, whereas the generating potential allows to concentrate the GSF basis set close to the origin while maintaining a realistic fall off behavior. It is usually in the inner region that the interacting part is important and needs a good numerical resolution. Thus, one may use the generating potential to tune the basis according to the particular physical problem under study.

2.3 Scattering states

For scattering solutions, one may set the full solution as⁷

$$\Psi(r) = \Psi_0(r) + \Psi_{sc}(r), \quad (21)$$

where $\Psi_0(r)$ is an asymptotic solution which solves a simplified, homogeneous, equation

$$\left[-\frac{1}{2\mu} \frac{d^2}{dr^2} + \frac{l(l+1)}{2\mu r^2} + V_0(r) - E \right] \Psi_0(r) = 0; \quad (22)$$

the scattering part $\Psi_{sc}(r)$ solves the inhomogeneous differential equation

$$\left[-\frac{1}{2\mu} \frac{d^2}{dr^2} + \frac{l(l+1)}{2\mu r^2} + V(r) - E \right] \Psi_{sc}(r) = -[V(r) - V_0(r)] \Psi_0(r). \quad (23)$$

Expanding $\Psi_{sc}(r)$ and $[V(r) - V_0(r)]\Psi_0(r)$ in Sturmian functions with externally fixed energy $E_s = E > 0$

$$\Psi_{sc}(r) = \sum_n a_n S_{nl}(r), \quad (24)$$

$$[V(r) - V_0(r)] \Psi_0(r) = \sum_n b_n \mathcal{V}(r) S_{nl}(r), \quad (25)$$

and using Eq. (2), the radial Schrödinger equation is converted into

$$\sum_n a_n [V(r) - \mathcal{U}(r) - \beta_{nl} \mathcal{V}(r)] S_{nl}(r) = - \sum_n b_n \mathcal{V}(r) S_{nl}(r). \quad (26)$$

Choosing again $\mathcal{U}(r) = V(r)$, only the generating potential remains on the LHS. Projecting to the left by $S_{n'l}(r)$, we end up again with a matrix problem

$$\beta_{n'l} a_{n'} = b_{n'}. \quad (27)$$

The Sturmian basis functions transform the operator $[H - E]$ into a diagonal matrix whose elements are simply the Sturmian eigenvalues. This can be seen in an alternative form. Equation (23) can be rewritten as:

$$\Psi_{sc}^{\pm}(r) = G_l^{\pm}[V(r) - V_0(r)]\Psi_0(r) \quad (28)$$

in terms of Green's function G_l^{\pm} which is responsible for providing the correct asymptotic behavior (outgoing (+) or incoming (-)) to $\Psi_{sc}^{\pm}(r)$. Now, Green's function satisfies the equation

$$\left[-\frac{1}{2\mu} \frac{d^2}{dr^2} + \frac{l(l+1)}{2\mu r^2} + V(r) - E \right] G_l^{\pm}(E, r, r') = \delta(r - r'), \quad (29)$$

and can be expanded in terms of Sturmian functions as follows:

$$G_l^{\pm}(E, r, r') = \sum_n g_{nl} S_{nl}^{\pm}(r') S_{nl}^{\pm}(r). \quad (30)$$

Replacing this expansion into (29), using Eq. (2), and taking $\mathcal{U}(r) = V(r)$, we find

$$-\sum_n g_{nl} \beta_{nl} S_{nl}^{\pm}(r') S_{nl}^{\pm}(r) \mathcal{V}(r) = \delta(r - r'). \quad (31)$$

Comparing this expression with the closure relation (5) we see that $g_{nl} = -1/\beta_{nl}$. This means that Green's function is diagonal in the Generalized Sturmian representation. Besides, the representation is optimized since the asymptotic region is associated with the range of the generating potential $\mathcal{V}(r)$; the asymptotic form of G_l^{\pm} is directly given by the correct asymptotic behavior of the Sturmian functions. Indeed, since (2) can be written as

$$-\frac{1}{\beta_{nl}} S_{nl}^{\pm}(r) = G_l^{\pm} \mathcal{V}(r) S_{nl}^{\pm}(r), \quad (32)$$

the Sturmian functions are eigenfunctions of the operator $G_l^{\pm} \mathcal{V}(r)$ with eigenvalues $-1/\beta_{nl}$.²⁵⁻²⁷

It is clear that for scattering problems, the Schrödinger equation to be solved is considerably simplified when using GSF.

2.3.1 Numerical implementation

As pointed out above, a detailed description of the numerical procedures has been presented in Ref. 43. In order to calculate the Sturmian functions suitable for scattering calculations, we set the boundary conditions by choosing

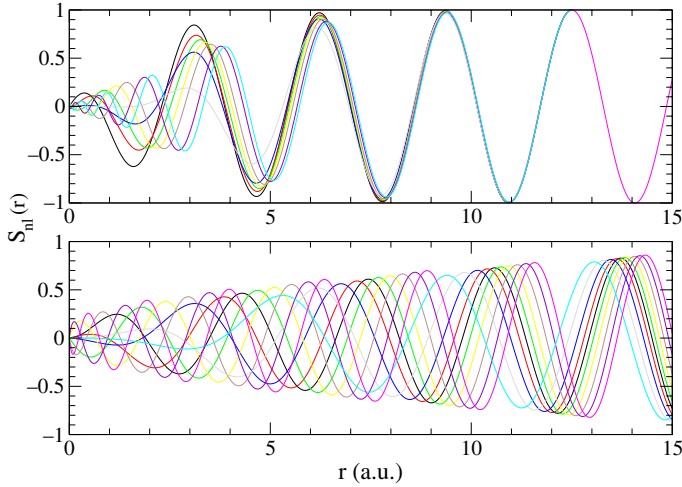


Figure 7.2 Up: First Generalized Sturmian functions S_{n0} for an auxiliary potential $\mathcal{U}(r) = 0$, a generating potential $\mathcal{V}(r) = e^{-0.375r}/r$, and an energy $E = 2.0$ a.u. Down: Coulomb Sturmian functions, for the same energy. For color version of this figure, the reader is referred to the online version of this chapter.

appropriately the auxiliary potential. For Coulombic outgoing/incoming boundary conditions, we calculate the regular $F(r)$ and irregular $G(r)$ radial Coulomb functions, and their derivatives, corresponding to a Sommerfeld parameter η . The asymptotic solution is then written as:

$$P(r \geq R_A) = \cos \delta F(r) + \sin \delta G(r). \quad (33)$$

where δ is the phase shift, calculated by assuming arbitrarily that at the point R_A the function satisfies $S_{nl}(R_A) = 1$, i.e.,

$$\begin{aligned} \cos \delta &= \frac{F(R_A) + iG(R_A)}{F(R_A)^2 + G(R_A)^2}, \\ \sin \delta &= \frac{G(R_A) - iF(R_A)}{F(R_A)^2 + G(R_A)^2}. \end{aligned} \quad (34)$$

In the same way as for the bound levels, the degree of mismatch of the solutions at the matching point allows estimation of the change $\Delta\beta_n$ needed for the next iteration step, until convergence is achieved in the slopes of the outward and inward functions.

As an example, consider the case in which $E = 2.0$ a.u. and $l = 0$, with the same auxiliary and generating potentials used in the previous bound state illustration. Figure 7.2 displays the first 10 GSF and, for comparison, the first 10 CSF corresponding to the same energy, and with outgoing

boundary conditions. For GSF, the role played by the two potentials is now clear: the generating potential $\mathcal{V}(r)$ is used to compress the basis inside the range of the interaction, while the auxiliary potential $\mathcal{U}(r)$ dictates the asymptotic behavior which, for the GSF, is unique for all basis elements.

This is in contrast with CSF which possess different asymptotic behaviors. It has to be noted also that the CSF with outgoing flux behavior are divergent unless the energy is appropriately chosen to be complex.

2.3.2 Example

An application of the GSF method is given by the following example in which we define a distorted wave approach to the Coulomb wave equation, with a Sommerfeld parameter $\eta = z_1 z_2 \mu / k$. Consider the asymptotic function $\Psi_0(r)$ of Eq. (21) as given by

$$\begin{aligned} \Psi_0(r) &= \sin \left[kr - \left(\eta \ln(2kr) + \frac{\pi}{2} l \right) g(r) \right] \\ &\xrightarrow{r \rightarrow \infty} \frac{1}{2i} \left(-e^{-i[kr - \eta \ln(2kr) - \frac{\pi}{2} l]} + e^{i[kr - \eta \ln(2kr) - \frac{\pi}{2} l]} \right), \end{aligned} \tag{35}$$

where $g(r)$ can be any function growing faster than r at the origin and tending to one at large distances as, e.g., $g(r) = 1 - e^{-a_c r}$ (a_c is a positive real constant). The function $\Psi_0(r)$ solves, asymptotically, the Schrödinger equation:

$$\left[-\frac{1}{2\mu} \frac{d^2}{dr^2} + \frac{l(l+1)}{2\mu r^2} + \frac{z_1 z_2}{r} - E \right] \Psi_0(r) = \mathcal{O} \left(\frac{1}{r^2} \right). \tag{36}$$

By using $\Psi_0(r)$ instead of the free-particle function $y_l(r)$ —the spherical Bessel function—we are introducing a distorted-wave approach.¹⁴ With these definitions the decomposition (21) is in agreement with standard scattering theory. Indeed, the driven Schrödinger equation to solve is

$$\begin{aligned} &\left[-\frac{1}{2\mu} \frac{d^2}{dr^2} + \frac{l(l+1)}{2\mu r^2} + \frac{z_1 z_2}{r} - E \right] \Psi_{sc}(r) \\ &= \left[E - \left(-\frac{1}{2\mu} \frac{d^2}{dr^2} + \frac{l(l+1)}{2\mu r^2} \right) - \frac{z_1 z_2}{r} \right] \Psi_0(r). \end{aligned} \tag{37}$$

According to Eq. (36), the RHS of (37) goes as $1/r^2$ at large distances, so that one may require $\Psi_{sc}(r)$ to have outgoing behavior $A_l e^{i[kr - \eta \ln(2kr) - \frac{\pi}{2} l]}$, as scattering theory establishes. One may then extract the corresponding transition amplitude since, at large distances, we have

$$\begin{aligned} \Psi^+(r) &\rightarrow \frac{1}{2i} \left(-e^{-i[kr - \eta \ln(2kr) - \frac{\pi}{2} l]} + e^{i[kr - \eta \ln(2kr) - \frac{\pi}{2} l]} \right) \\ &+ A_l e^{i[kr - \eta \ln(2kr) - \frac{\pi}{2} l]}, \end{aligned} \tag{38}$$

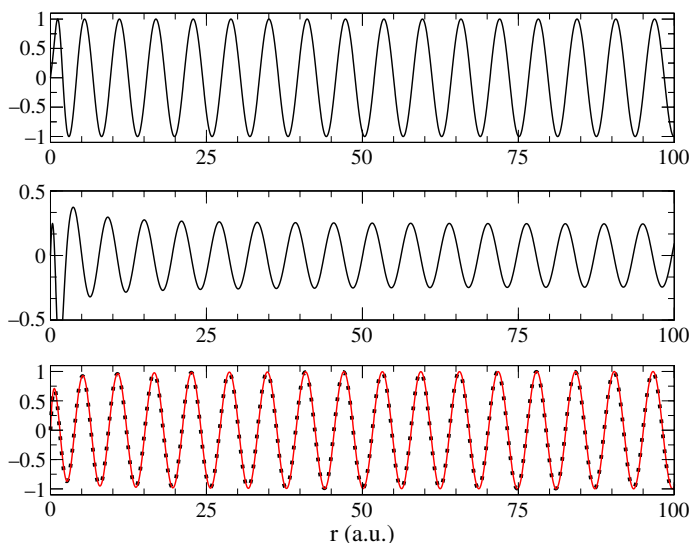


Figure 7.3 The functions $\Psi_0(r)$ (top panel), $\Psi_{sc}(r)$ (middle panel), and $\Psi(r)$ (bottom panel) of, respectively, Eqs. (35), (37), and (21) are plotted as a function of the radial coordinate r ; we have taken $l = 0, k = 1, \mu = 1$, and $z_1 z_2 = -1$, and $a_c = 0.5$ in Eq. (35). In the bottom panel, the Coulomb wave function $F(r)$ is included (solid dots) for comparison. For color version of this figure, the reader is referred to the online version of this chapter.

where the transition matrix $A_l = e^{i\delta_l} \sin(\delta_l)$ will result from solving Eq. (37) for $\Psi_{sc}(r)$.

To illustrate the proposal, the distorted-wave driven Eq. (37) was solved numerically using GSF with outgoing asymptotic behavior.¹⁴ In the top and middle panels of Figure 7.3, we plot the functions $\Psi_0(r)$ and $\Psi_{sc}(r)$. In the bottom panel the sum of these functions, $\Psi(r)$, as defined in Eq. (21) is shown and compared with the exact Coulomb wave function $F(r)$ (solid dots) with unit asymptotic norm. The facts that $\Psi_0(r)$ possesses the appropriated Coulomb distortion and that the sum (21) leads to the correct result, show that the driven Eq. (37) is well formulated and is in accordance with scattering theory.



3. THREE-BODY PROBLEMS: BOUND STATES

The configuration interaction method has been widely used to perform *ab initio* calculations of N -electron atomic and molecular systems.^{5,17–19,48,49} The differences between various implementations reside in the type of radial basis set used to expand the solutions. The great

advantage of the *CI* method is its simplicity and flexibility. It allows *ab initio* calculations of three or more particle systems in a relatively easy way. However, the convergence rate is strongly dependent on the quality of the chosen basis functions.

Among the many basis sets in spherical coordinates, a very efficient scheme for atomic systems is based on the use of Laguerre-type orbitals⁴⁸ which essentially define the Coulomb Sturmian functions. The parameters of the CSF basis for two-electron systems are numerically optimized to obtain the best values for the energies.⁴⁹ This Sturmian methodology was shown to be efficient in obtaining atomic bound states for two- and three-electron atoms, as well as for molecular systems.

Here we present an alternative *CI* methodology based on two-body GSF selecting parameters to construct optimized basis functions for bound state problems.

3.1 Systems with general masses

Let us consider three particles with masses (m_1, m_2, m_3) and charges (z_1, z_2, z_3) , where m_3 is the heaviest particle. Separating the center of mass motion, and denoting by \mathbf{r}_1 and \mathbf{r}_2 the relative coordinates of particles m_1 and m_2 with respect to m_3 , the Hamiltonian describing the relative motion of the two lighter particles is written as:

$$H = -\frac{1}{2\mu_{13}}\nabla_{\mathbf{r}_1}^2 - \frac{1}{2\mu_{23}}\nabla_{\mathbf{r}_2}^2 - \frac{1}{m_3}\nabla_{\mathbf{r}_1} \cdot \nabla_{\mathbf{r}_2} + \frac{z_1 z_3}{r_1} + \frac{z_2 z_3}{r_2} + \frac{z_1 z_2}{r_{12}}, \quad (39)$$

where $\mu_{ij} = (m_i m_j)/(m_i + m_j)$ is the reduced mass of particle i with respect to particle j , $r_{12} = |\mathbf{r}_1 - \mathbf{r}_2|$ and the operator $-\frac{1}{m_3}\nabla_{\mathbf{r}_1} \cdot \nabla_{\mathbf{r}_2}$ is the mass polarization term. The wave function $\Psi(\mathbf{r}_1, \mathbf{r}_2)$ satisfies the Schrödinger equation

$$H\Psi(\mathbf{r}_1, \mathbf{r}_2) = E\Psi(\mathbf{r}_1, \mathbf{r}_2), \quad (40)$$

where E is the energy of the three-particle system.

We may define the *CI* expansion of the wave function using two-body GSF for each coordinate \mathbf{r}_1 and \mathbf{r}_2 . For a given total angular momentum L and projection M , it is written as:

$$\Psi(\mathbf{r}_1, \mathbf{r}_2) = \sum_{l_1 l_2} \sum_{n_1=1}^{N_1} \sum_{n_2=1}^{N_2} a_{n_1 n_2}^{l_1 l_2 LM} \mathcal{A} \frac{S_{n_1 l_1}(r_1)}{r_1} \frac{S_{n_2 l_2}(r_2)}{r_2} \mathcal{Y}_{l_1 l_2}^{LM}(\hat{\mathbf{r}}_1, \hat{\mathbf{r}}_2), \quad (41)$$

where $a_{n_1 n_2}^{l_1 l_2 LM}$ are the expansion coefficients and $\mathcal{A} = (1 + \epsilon P_{12})/\sqrt{2}$ is the symmetrization operator that accounts for the exchange of the particles.

The permutation operator P_{12} exchanges coordinates $r_1 \leftrightarrow r_2$, and $\epsilon = 1$ for singlet states or $\epsilon = -1$ for triplet states.

The angular part is expressed in terms of the coupled spherical harmonics¹

$$\mathcal{Y}_{l_1 l_2}^{LM}(\hat{\mathbf{r}}_1, \hat{\mathbf{r}}_2) = \sum_{m_1 m_2} \langle l_1 m_2 l_2 m_2 | l_1 l_2 LM \rangle Y_{l_1 m_1}(\hat{\mathbf{r}}_1) Y_{l_2 m_2}(\hat{\mathbf{r}}_2), \quad (42)$$

where Y_{lm} are spherical harmonics and $\langle l_1 m_2 l_2 m_2 | l_1 l_2 LM \rangle$ are Clebsch-Gordan coefficients. The individual angular momenta l_1 and l_2 must satisfy the triangular rule and parity conservation $(-1)^L = (-1)^{l_1+l_2}$. To avoid redundancies in expansion (41), the angular momenta are restricted to $l_1 \leq l_2$. Also, if $l_1 = l_2$, then $n_1 \leq n_2$. These restrictions ensure numerical stability in the calculation, avoiding repeated sets of equations given by symmetry.

Replacing expansion (41) into the Schrödinger Eq. (40) and projecting onto the Sturmian basis set, we obtain a generalized eigenvalue problem of the form

$$\mathbf{H} \mathbf{a}_\nu^{LM} = E_\nu \mathbf{S} \mathbf{a}_\nu^{LM}, \quad (43)$$

where for a given state ν , the vector \mathbf{a}_ν^{LM} contains the expansion coefficients $a_{n_1 n_2}^{l_1 l_2 LM}$ for fixed (L, M) . The energy eigenvalues are $E = E_\nu$, while the Hamiltonian and overlapping matrices \mathbf{H} and \mathbf{S} have elements

$$[\mathbf{H}]_{n_1' n_2' n_1 n_2}^{LM l_1' l_2' l_1 l_2} = \left\langle \mathcal{Y}_{l_1' l_2'}^{LM} \frac{S_{n_1' l_1'}}{r_1} \frac{S_{n_2' l_2'}}{r_2} \middle| H \middle| \mathcal{A} \frac{S_{n_1 l_1}}{r_1} \frac{S_{n_2 l_2}}{r_2} \mathcal{Y}_{l_1 l_2}^{LM} \right\rangle, \quad (44)$$

$$[\mathbf{S}]_{n_1' n_2' n_1 n_2}^{LM l_1' l_2' l_1 l_2} = \left\langle \mathcal{Y}_{l_1' l_2'}^{LM} \frac{S_{n_1' l_1'}}{r_1} \frac{S_{n_2' l_2'}}{r_2} \middle| \mathcal{A} \frac{S_{n_1 l_1}}{r_1} \frac{S_{n_2 l_2}}{r_2} \mathcal{Y}_{l_1 l_2}^{LM} \right\rangle. \quad (45)$$

The matrices \mathbf{H} and \mathbf{S} can be computed as:

$$\begin{aligned} [\mathbf{H}]_{n_1' n_2' n_1 n_2}^{LM l_1' l_2' l_1 l_2} &= \left[(E_1 + E_2) O_{n_1' n_1}^{l_1' l_1} O_{n_2' n_2}^{l_2' l_2} - \beta_{n_1 l_1} [\mathcal{V}_1]_{n_1' n_1}^{l_1' l_1} O_{n_2' n_2}^{l_2' l_2} \right. \\ &\quad \left. - \beta_{n_2 l_2} [\mathcal{V}_2]_{n_2' n_2}^{l_2' l_2} O_{n_1' n_1}^{l_1' l_1} \right] \delta_{l_1' l_1} \delta_{l_2' l_2} \\ &\quad + [\mathbf{T}_{12}]_{n_1' n_2' n_1 n_2}^{LM l_1' l_2' l_1 l_2} + \sum_{l=0}^{\infty} \frac{4\pi}{2l+1} R_{n_1' n_2' n_1 n_2}^{l_1' l_2' l_1 l_2 l} \sum_{m=-l}^l A_{l_1' l_2' l_1 l_2}^{LM} \\ &\quad + \epsilon P(n_1 \rightarrow n_2, l_1 \rightarrow l_2), \end{aligned} \quad (46)$$

$$[\mathbf{S}]_{n_1' n_2' n_1 n_2}^{LM l_1' l_2' l_1 l_2} = O_{n_1' n_1}^{l_1' l_1} O_{n_2' n_2}^{l_2' l_2} \delta_{l_1' l_1} \delta_{l_2' l_2} + \epsilon P(n_1 \rightarrow n_2, l_1 \rightarrow l_2). \quad (47)$$

For the sake of compactness, we do not provide here explicit expressions for the mass polarization matrix \mathbf{T}_{12} . Nine different terms are necessary to calculate it with no evaluation difficulties. For the electron–electron interaction term use is made of the standard spherical harmonics expansion

$$\frac{1}{r_{12}} = \sum_{l=0}^{\infty} \sum_{m=-l}^l \frac{4\pi}{2l+1} \frac{r_{<}^l}{r_{>}^{l+1}} Y_{lm}^*(\theta_1, \phi_1) Y_{lm}(\theta_2, \phi_2), \quad (48)$$

with $r_{<} = \min(r_1, r_2)$ and $r_{>} = \max(r_1, r_2)$. In the matrix expressions (46) and (47) we explicitly noted the action of the operator $P_{12} = P(n_1 \rightarrow n_2, l_1 \rightarrow l_2)$ onto the index of the basis set, and defined the following integrals:

$$O_{n'n}^{l'l} = \int_0^{\infty} dr S_{n'l'}(r) S_{nl}(r), \quad (49a)$$

$$[\mathcal{V}_i]_{n'n}^{l'l} = \int_0^{\infty} dr S_{n'l'}(r) \mathcal{V}_i(r) S_{nl}(r), \quad (49b)$$

$$R_{n_1' n_2' n_1 n_2}^{l_1' l_2' l_1 l_2} = \int_0^{\infty} dr_1 \int_0^{\infty} dr_2 S_{n_1' l_1'}(r_1) S_{n_2' l_2'}(r_2) \frac{r_{<}^l}{r_{>}^{l+1}} S_{n_1 l_1}(r_1) S_{n_2 l_2}(r_2), \quad (49c)$$

$$A_{l_1' l_2' l_1 l_2}^{LM} = \int d\hat{\mathbf{r}}_1 \int d\hat{\mathbf{r}}_2 \mathcal{Y}_{l_1' l_2'}^{LM*}(\hat{\mathbf{r}}_1, \hat{\mathbf{r}}_2) Y_{lm}^*(\hat{\mathbf{r}}_1) Y_{lm}(\hat{\mathbf{r}}_2) \mathcal{Y}_{l_1 l_2}^{LM}(\hat{\mathbf{r}}_1, \hat{\mathbf{r}}_2). \quad (49d)$$

3.2 Two-electron atoms

We first look at the case where the two light particles are electrons ($m_1 = m_2 = 1, z_1 = z_2 = -1$) bound to a heavy nucleus of infinite mass ($m_3 \rightarrow \infty$), so the mass polarization term can be omitted

$$H_a = -\frac{1}{2\mu_{13}} \nabla_{\mathbf{r}_1}^2 - \frac{1}{2\mu_{23}} \nabla_{\mathbf{r}_2}^2 + \frac{z_1 z_3}{r_1} + \frac{z_2 z_3}{r_2} + \frac{z_1 z_2}{r_{12}}. \quad (50)$$

We test our method computing the ground state of He ($z_3 = 2$) and H^- ($z_3 = 1$), and then extend our study to singly and doubly excited states of He.

The GSF for each electron can be defined for different sets of basis parameters ($\mathcal{U}(r), \mathcal{V}(r), E, N$). Our basis can represent either symmetric states where the electrons are equivalent (such as the ground state) or

asymmetric excited states, where one electron has a lower energy than the other. Different basis parameters may be convenient to deal with continuum (for example, auto-ionizing) states. In all cases, we will use the notation E_i and N_i for $i = 1, 2$ to distinguish the electrons.

So far, we have considered the energy of the basis set as a real, negative parameter, so the GSF have an exponentially decaying asymptotic behavior. However, if the energy is chosen to be positive, outgoing wave asymptotic behavior can be imposed to the basis set, which is adequate for doubly excited, auto-ionizing states. The matrix obtained with this boundary condition is now complex symmetric and non-Hermitian, and the eigenvalues will be complex, too.

3.2.1 Partial-wave analysis of the ground state of He and H^-

In Table 7.1, we show the ground-state energy of He as a function of the angular configurations (l_1, l_2) considered for each electron. These results are, as far as we know, the best obtained with uncorrelated basis.^{38,42} They were obtained with 20 GSF per angular momentum quantum number l_i , with a generating Yukawa potential with $a_s = 0.375$ and $E_i = -1.48385$ a.u. ($i = 1, 2$). The calculation was performed up to $l_1 = l_2 = 12$, for which the maximum basis size was $N_{tot} = 2520$. We compare our results with those of Fomouo and collaborators⁹ (obtained with 40 radial CSF functions per l_i for each electron) and with those of Bromley and Mitroy⁴⁹ (obtained with 20 radial functions per l_i for each electron). In these studies, a symmetric basis was used, composed of products of Laguerre-type orbitals with special choices of the scaling parameter λ . In the work of Fomouo, that parameter is fixed to a particular value, while in the work of Bromley it is varied

Table 7.1 Partial-wave analysis of the He ground state. l_i ($i = 1, 2$) is the maximum angular configuration (l_1, l_2) considered. The second and third columns show calculations with 20 GSF and CSF per l_i , respectively, while the fourth column uses 40 CSF

l_i	He ground-state energy		
	GSF ³⁸	CSF ⁴⁹	CSF ⁹
0	-2.879 028 654	-2.879 028 507 ($\lambda = 4.8$)	-2.879 027 97
1	-2.900 515 957	-2.900 515 873 ($\lambda = 7.8$)	-2.900 513 86
12	-2.903 710 272	-2.903 711 927 ($\lambda = 25.5$)	-
Exact ⁵⁰	-2.903 724 377		

independently for each l_i (almost 12 variational parameters for the best value obtained with 20 single-electron orbitals per l_i for $l_i = 12$). In both cases the use of Laguerre basis functions implies that the asymptotic behavior of the basis is not the one associated to the state that they are expanding, since the Coulombic logarithmic phase associated to CSF changes from one basis element to the other. This is not the case of GSF basis set where all the elements have the same asymptotic behavior, both exponential factor and power law. The asymptotic region does not need to be expanded with our basis, since it is already included exactly in all basis elements.

Note that optimizing only one parameter for the case $l_i = 0$, GSF give better results than those of Bromley and Mitroy for $l_i = 0$. Our result obtained with l_i up to 12 is compared with those of Fomouou and co-workers. The energy values presented in the table show that we have obtained more accurate results using half of the coefficients required by Fomouou. To obtain better values for l_i up to 12 we have to perform an optimization over a_s . We found that this optimization was not sufficient to reproduce Bromley's accuracy: we thus also varied the energy of the GSF basis. We found that by setting $a_s = 0.795$ and $E = 1.05$ a.u. for the 12 angular momenta, the resulting energy -2.903712009 a.u. is in better agreement with the exact value than any other calculations. Note also that this last calculation was performed adjusting both the asymptotic behavior of the basis set as well as the region where the He ground state is defined. The optimization of these two physical basis parameters is enough to avoid the complete optimization procedure (involving 13 parameters λ) implemented by Bromley and Mitroy.

Within the GSF method, the above calculation is relatively straightforward. However, the basis functions can be optimized even further to include more physics of the problem,⁴² improving both their short distance and their asymptotic behavior. It is known that when one of the electrons is far from the nucleus, it is screened by the other, inner, electron. This can be associated to an effective charge "seen" by the outer electron. For that purpose we define the auxiliary potential as:

$$U(r) = -\frac{Z_{as}}{r} + \frac{(-Z_{in} + Z_{as})e^{-a_s r}}{r}. \quad (51)$$

In many-electron wave function expansions, Z_{in} could be, for example, optimally chosen to be the electron-nucleus interaction weight, and Z_{as}

the asymptotic averaged charge of the electron in its outer region: i.e., $Z_{as} = Z_{in} - (N - 1)$, where N is the number of electrons.

Since the GSF equation includes both the generating and auxiliary potential, the Coulomb properties associated to $\mathcal{U}(r)$ should not be lost by the choice of $\mathcal{V}(r)$ either at $r \rightarrow 0$ or $r \rightarrow \infty$. An adequate selection is

$$\mathcal{V}(r) = -\frac{e^{-\lambda r}}{r} \left[r^\delta e^{-\gamma r^2} + (1 - e^{-\gamma r^2}) \right], \quad (52)$$

with $\lambda > 0$, $\delta > 0$, and $\gamma > 0$. In this way, there are no further Coulomb singularities at $r \rightarrow 0$ nor logarithmic distortion at $r \rightarrow \infty$ apart from those associated to $\mathcal{U}(r)$. This fulfills the electron–nucleus Kato cusp conditions (see Ref. 42, for a more detailed description). With such basis functions we first performed a variational calculation for $l_i = 0$. This allowed us to obtain values for all the parameters of the potential $\mathcal{V}(r)$ and the parameter a_{tr} of the potential $\mathcal{U}(r)$. Then, we further improved the calculations with l_i up to 12 by adjusting E_i and λ . The values of the parameters are $E_i = -1.05$, $Z_{in} = -2$, $Z_{as} = -2$, $a_{tr} = 0$, $\lambda = 0.93$, $\delta = 0.3$, and $\gamma = 4$. With these values we obtained a ground-state energy of -2.903712820 a.u. for $l_i = 12$ and with 455 basis functions.

A similar calculation has been performed for H^- ,⁴¹ with 40 GSF for each electron per l_i , up to $l_i = 5$, obtaining a ground-state energy equal to $E_0 = -0.52772866$ a.u., in excellent agreement with the very precise variational result $E_0 = -0.52775101635$ a.u., given by Freund et al.⁵¹

3.2.2 Singly-and doubly excited states of He

We extend our study to calculate energies of asymmetrical (excited) states.⁵² The improvement in accuracy and convergence reached in comparison with previous calculations is shown in Table 7.2 for the singlet and triplet states of He for $L = 3$. The size of the Sturmian basis for each electron is much smaller compared to that of the ground state, and few angular momenta configurations are needed to achieve convergence. The basis parameters are now different for each electron with $E_1 = -1.95$ a.u., $E_2 = -0.1$ a.u., $a_{s1} = 0.1$, $a_{s2} = 0.3$ and the one-electron basis sizes are $N_1 = 2$ and $N_2 = 12$. The same parameters were used for singlet and triplet cases.

In Table 7.3, we show the results for singly excited states of He with different values of angular momentum L and levels n . The energy values obtained were optimized first for the lowest n level. Although the basis parameters are those which give the best lower energy, they provide a good

Table 7.2 Convergence of the 4^1F and 4^3F He state energy as a function of the electron pair of angular momenta

l_1, l_2	Size	4^1F	4^3F
(0,3)	24	-2.031249	-2.031250
(1,2)	48	-2.031252256	-2.031252292
(2,3)	96	-2.03125509730	-2.03125511983
(3,4)	144	-2.03125512818	-2.03125514924
Ref. 57		-2.03125514438175	-2.03125516840324

Table 7.3 Energy of the first three excited states for singlet states of He for different L with a total of 168 basis functions

n	L	Present work	Ref. 57
3	2	-2.0556110426	-2.0556207328522456
4	3	-2.03125512987	-2.0312551443817490
5	4	-2.020000709670	-2.0200007108985847
6	5	-2.0138890317669	-2.0138890347542797

representation of the excited energy states as well. Of course this can be improved by changing the basis set values of the energy or the range of the Yukawa potential. However, we want to emphasize that the discretization provided by the finite spectral representation gives a good approximation for the lowest excited states without increasing the size or changing the basis set for each state under scrutiny.

Finally, we would like to point out that the precision of our values increases for higher total angular momenta. As mentioned before, the energies of the asymmetrical states are expected to give better accuracy than those of the ground states for the same number of basis elements. This is confirmed by our calculations.

Up to this point, we have shown that our method is able to deal with the ground and asymmetrical states for two-electron systems, for which exponential decay is the suitable asymptotic behavior. Our method can also be applied to calculate the doubly excited states of a two-electron atom. To this end, we choose a positive energy for the Sturmian basis, and the asymptotic behavior as outgoing wave, to meet the requirements of the doubly excited states where one of the electrons can escape and move far

Table 7.4 Energies for the Rydberg series of the singlet S states of He, using 30 GSF per electron

$(N, k)_n$	GSF		Ref. 58	
	$\Re(E)$	$\Im(E)$	$\Re(E)$	$\Im(E)$
$(2, 1)_2$	-0.777876955	-0.002060106	-0.777867636	-0.002270653
$(2, -1)_2$	-0.621817695	-0.000106535	-0.621927254	-0.000107818
$(3, 2)_3$	-0.351827523	-0.001406250	-0.353538536	-0.001504906

from the nucleus. The He eigenvalues E_i obtained with the diagonalization are then complex: the real part is the energies of each atomic state, while the imaginary one gives the width of the state lines. The choice of the basis parameters is made in a similar fashion as for the ground state, but the basis size must be increased for good accuracy.

In Table 7.4, we present the results for the real and imaginary part of the energy for some of the singlet S states of He. We use the $(N, k)_n$ nomenclature for the Rydberg series: the index N denotes the principal quantum number of the remaining ion once the outer electron is ionized. The index n denotes the principal quantum number of the outer electron while the index k determines the parabolic quantum number of the Stark-type state in which the inner electron resides.

The basis set parameters were chosen to give the best value of the first doubly excited state but note that good results for other states can be achieved. The size of the basis set can be increased not only to obtain more accurate results but also to find more eigenvalues that correspond to the Rydberg series.

Remarkable calculations have been performed by Piraux and collaborators using uncorrelated basis.^{53–56} Using CSF, they obtained singly and doubly excited states comparable with the results provided by Drake with correlated basis functions. The advantage observed in their method is that the calculations required only one diagonalization and very few non-linear parameters. States with no natural parity were also studied with great success.^{54,55}

3.3 Finite mass exotic and molecular systems

We shall now show that the CI approach with GSF is quite versatile, as it can be applied to any set of three particles, atomic or molecular. For bound states, we shall briefly consider several situations: two light particles of equal ($[\mu^-, \mu^-, {}^3\text{He}^{+2}]$) or unequal masses (muonic helium: $[e^-, \mu^-, \text{He}^{+2}]$),

Table 7.5 Ground-state energy of the $[\mu^-, \mu^-, {}^3\text{He}^{+2}]$ system. We used 20 radial functions per coordinate and for each partial-wave l_i

$[\mu^-, \mu^-, {}^3\text{He}^{+2}]$ Ground-state energy	
l_i	E_{l_i}
0	-576.874 110
4	-577.555 143
...	...
20	-577.593 497
Refs. 59,60	-576.934 471

three light particles (the Ps^- system), and two heavy particles with a light one (H_2^+).

3.3.1 Ground state of the $[\mu^-, \mu^-, {}^3\text{He}^{+2}]$ system

Consider a three charged particle atom with $z_1 = z_2 = -1$ and $z_3 = 2$, $m_3 = 5495.8852$ a.u. and $m_1 = m_2 = m_\mu$, where m_μ is the muon mass equal to 206.768262 a.u. Since the muons are heavy particles, they will remain much closer to the atomic nucleus than in the case of two electrons. In the calculations presented here we describe the muon–nucleus pairs with GSF which are defined on a radial domain of 0.050 a.u. and with basis energy $E = -300$ a.u. Table 7.5 shows our Sturmian expansion partial-wave results compared with the value given by Rodriguez et al.^{59,60} obtained with a modest number of correlated basis functions.

3.3.2 Ground states of the $[\mu^-, e^-, {}^A\text{He}^{+2}]$ systems

Now we consider a He-like system where only one electron is replaced by a muon. This is a very asymmetrical system due to the difference between each particle's mass. Moreover, we consider two different nuclear masses of ${}^A\text{He}^{+2}$: $A = \infty$ and $A = 3$. As already mentioned, the muon–nuclei subsystem maintains a very short separation compared to the electron–nucleus pair. This produces a screening of the nuclear charge seen by the electron. We employed different GSF basis to describe the dynamics of the $\mu^- - \text{He}^{+2}$ and $e^- - \text{He}^{+2}$ pairs, defined over radial regions equal to 0.025 and 15 a.u., respectively. The results were not so sensitive to the variation of the rest of the parameters appearing in the Sturmian equation. For these three-body

Table 7.6 Ground state energy of the $[\mu^-, e^-, {}^A\text{He}^{+2}]$ systems. We used 20 radial functions per coordinate and for each partial-wave l_j

$[\mu^-, e^-, {}^A\text{He}^{+2}]$ Ground-state energy		
l_j	$A = \infty$	$A = 3$
2	-414.036 397	-399.041 527
Refs. 59,60	-414.036 395	-399.042 262

systems the partial wave convergence is very fast; we present in Table 7.6 only the $l_j = 2$ calculations and compare with the results of Refs. 59,60.

3.3.3 Ground state of the Ps^- system

We consider now the Ps^- three-body system, which corresponds to $z_1 = z_2 = -1$ and $z_3 = 1$, and to reduced masses $\mu_{13} = \mu_{23} = 0.5$. Since now $m_3 = 1$ is finite, the mass polarization term will play an important role in the Hamiltonian (39), unlike in the previous two atomic systems. We have used the same generating and auxiliary potentials of Eqs. (51) and (52) with the following parameters: $E_s = -0.06371$, $Z_{in} = Z_{as} = -1$, $\alpha = 1$, $\lambda = 0.1$, $\delta = 0.3$, and $\gamma = 4$. As in the previous systems, this calculation is not fully variational. By

Table 7.7 Partial-wave convergence of the ground-state energy of Ps^- system. We used 35 radial functions per coordinate and for each partial-wave l_j

Ps^- Ground-state energy	
l_j	E_{l_j}
0	-0.257 240 143
1	-0.260 105 390
2	-0.261 496 276
...	...
12	-0.262 002 458
Exact ⁶¹	-0.262 005 070

adjusting λ and the basis energy, including partial-waves up to $l_i = 6$ is enough to reach energy values below -0.262 a.u. Our best energy value (see Table 7.7), obtained considering up to $l_i = 12$, is in excellent agreement with the very accurate results of Drake et al.⁶¹

3.3.4 Ground state of H_2^+

Finally, we consider the molecular three-body system H_2^+ . As we now have two heavy particles, there is no natural assignment for particle 3. By taking it to be one of the protons, we have $z_1 = z_3 = 1$ and $z_2 = -1$, and the reduced masses $\mu_{13} = m_p/2$ and $\mu_{23} \simeq 1$. Since $m_3 = m_p$ is finite, the product of gradient operators will play an important role in Eq. (39). Alternatively, exploiting the symmetry, we may take the electron as particle 3; in this case, $z_1 = z_2 = 1$ and $z_3 = -1$, and $\mu_{13} = \mu_{23} \simeq 1$. With this latter choice, the Schrödinger equation (39) does not differ too much from that of H^- , except by the mass polarization term, the center of coordinates being different. We emphasize that we do not consider the Born–Oppenheimer approximation in either case, as we treat the three particles in a fully quantum framework. Results are shown in Table 7.8.

3.4 Confined atoms

Scientists have paid much attention to the study of atoms and molecules under different compression regimes. This is due to the existence of diverse situations in physics and chemistry such as atoms trapped in cavities, in zeolite channels, or encapsulated in hollow cages of carbon-based

Table 7.8 Partial-wave convergence of the ground-state energy of H_2^+ molecule. We used 35 radial functions per coordinate and for each partial-wave l_i , except for $l_i = 0$ for which we used 44 functions per coordinate

H_2^+ Ground-state energy	
l_i	E_{l_i}
0	−0.513 721 047
2	−0.560 413 338
...	...
20	−0.596 299 557
Exact ⁶²	−0.597 139 063

nano-materials such as endohedral fullerenes. Models of confined atomic and molecular systems have also found applications in the analysis of the so-called artificial atoms or quantum dots due to their relevance in technological applications. The spherically enclosed atoms represent a model that has been applied in the analysis of several confined systems with different methodologies where compression is simulated through hard or soft walls.

As an example of the versatility and precision of our GSF method we present two calculations of an He atom confined by external potentials. In the first case, the He atom is confined inside a penetrable cage, like a fullerene molecule. In the second case, we study the He confined by an infinite potential well.

3.4.1 He confined in endohedral fullerene

Fullerene molecules are capable of enclosing atoms in their hollow interior, forming endohedrally confined atoms. Since these systems can lead to important applications, we devoted a paper⁶³ analyzing the dependence of the He energy levels on the strength of the confining potential. It is expected that the atomic properties of the confined atom (such as the wave functions, energy levels, the filling of electronic shells, polarizability, photo-absorption, and ionization, etc.) will be dramatically changed both quantitatively and qualitatively, from those characteristic of the free atoms, and change the physical processes where these species are involved (see, for example, Ref. 64). As the goal was to obtain a general qualitative understanding of these effects, instead of dealing with the real helium atom, the authors calculated the spectra of the Helium atom within the spherically symmetric model (Temkin–Poet model). A further simplification was made by modeling the endohedral environment by an attractive short-range spherical shell with a potential

$$U(r) = \begin{cases} -U_0 < 0 & r_c \leq r \leq r_c + \Delta \\ 0 & \text{otherwise} \end{cases} \quad (53)$$

where r_c is the inner radius and Δ its thickness. The values deduced by Xu et al.⁶⁵, $r_c = 5.75$ a.u. and $\Delta = 1.89$ a.u., which are specific for a C_{60} fullerene molecule were considered. The value of U_0 , on the other hand, was varied from 0 to 10 a.u., in order to explore the general physics of the system, relevant to find other means of confining the atom (e.g., altering the number of carbon atoms in the fullerene cage). By varying the

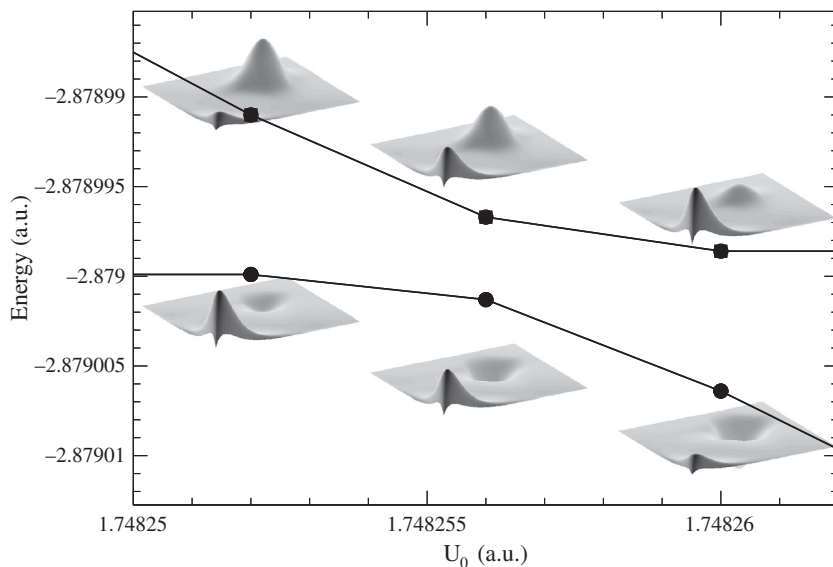


Figure 7.4 ψ_{1s^2} (He ground state) and ϕ_1^2 (two electrons in the fullerene cage) wave functions for different potential depths U_0 .

external confinement potential of an endohedrally confined hydrogen atom, Connerade et al.⁶⁶ studied the phenomenon of “mirror collapse”. This effect occurs when an electron bound by the Coulombic potential falls into the outer potential well, but, at the same time, an excited level, having a bound orbital extended over the outer shell, collapses into the inner Coulombic attraction corresponding to the first level.

The investigation of a similar effect for endohedrally confined He was found to be extremely difficult, because the mirror collapse positions in terms of the confining potential are amazingly evasive. In order to catch the exact point at which the collapse occurs one needs a very fine tuning of the potential strength. As an example, we can see, in Figure 7.4, the way in which two different electron configurations interact. In this case, one wave function (ψ_{1s^2}) represents the two He electrons in the ground state (since it is an S -wave model, its energy is -2.879 a.u.). The other wave function corresponds to the two electrons confined inside the fullerene cage (ϕ^2). The energy is strongly dependent on the confinement potential and, at some particular value, a crossing between ψ_{1s^2} and ϕ^2 must occur, and the corresponding mirror collapse of the wave functions may be observed.

In order to capture the precise point at which the mirror collapse occurs, many calculations of the He spectra are needed, one for each confinement

potential strength. It is necessary, therefore, to use a computational method capable of very fast calculations. Moreover, as Figure 7.4 shows, the collapse is extremely sensitive to the potential value. In this particular case, the effect occurs in a potential range between $U_0 = 1.74825$ and $U_0 = 1.74826$ a.u.. Thus, the computational method must also be very precise. Our GSF method is able to fulfill with both requirements.

3.4.2 He confined in an impenetrable spherical cage

Another example is the calculation of the atomic structure of an He atom inside an infinite potential well located at a given radius R . Many theoretical studies have been devoted to the effect of the confinement on atomic spectra. In particular, it has been observed that the degeneracy and relative ordering of the energy levels are both influenced significantly by the effect of confining potentials. Recently, considerable theoretical efforts have been made in performing more accurate computations on simple model systems, involving the hydrogen and helium atom, which could also serve as a benchmark for approximate methods. Within our GSF method, such calculations are straightforward. We only need to impose the confinement condition on the basis set, which automatically imposes the same condition on the total wave functions.

The spectrum of the He atom confined in a spherical cage of radius R is shown in Figure 7.5. In Table 7.9, the ground-state energies are shown as a function of the confinement radius R , and compared with

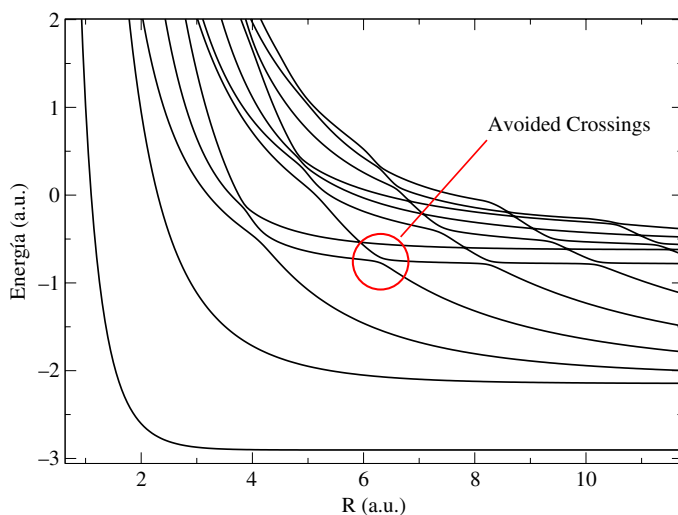


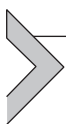
Figure 7.5 Confined He energies as a function of the cage radius R . For color version of this figure, the reader is referred to the online version of this chapter.

Table 7.9 Energies of the ground state of the confined He atom for different values of the confinement radius R

R	Present work	Ref. 68	Ref. 67	Ref. 71
0.6	13.318157	13.318340	13.3343	—
1.0	1.015794	1.015870	1.0183	1.0142
1.5	-1.906938	-1.906740	-1.9061	-1.9081
2.0	-2.604013	-2.603630	-2.5998	-2.6051
3.0	-2.872474	-2.871808	-2.8636	-2.8727
3.5	-2.893574	-2.892808	-2.8851	-2.8935
4.0	-2.900465	-2.899687	-2.8931	-2.9003
5.0	-2.903390	-2.902813	-2.8978	-2.9032
6.0	-2.903673	-2.903278	-2.8990	-2.9035
$R \rightarrow \infty$	-2.903712	-2.903513	-2.8999	-2.9037
Exact $R \rightarrow \infty$ ⁵⁰	-2.903724			

other calculations. Those of Banerjee et al.⁶⁷ have been obtained using a basis with two variational parameters. The calculations of Aquino et al.⁶⁸ used generalized Hylleras functions, and Joslin and Goldman⁷¹ performed Quantum Monte Carlo calculations, considered as the best available data values. Our calculations include up to the fifth partial wave and 20 radial functions per coordinate.

By linear interpolation one estimates the value of the critical cage radius at which the ground state crosses the $E = 0$ value. We found a value $R_c = 1.101125$ a.u., which is in very good agreement with the value $R_c = 1.1011$ a.u. obtained by Aquino.⁶⁸



4. THREE-BODY PROBLEMS: SCATTERING STATES

4.1 Introduction

The calculation of scattering states (subscript sc) is much more difficult than that of bound states; while this is true also for the two-body case, it is even more complicated for the three-body case. As we shall see in the next subsection, the presence of different channels is one of the major difficulties. Another aspect that will immediately appear is that hyperspherical coordinates are more natural in the asymptotic domain where the three particles are well separated.

For the two-body case, *vide infra*, one of the advantages of using GSF is that they allow to successfully impose correct asymptotic scattering

conditions. For the three-body case, the same strong statement cannot be made. The purpose of this section is to provide the theoretical Generalized Sturmian approach to solve three-body scattering problems. According to the channel one wants to study one of the two following expansions could be considered. The first one (essentially Eq. (41)) uses spherical coordinates, and is based on an adequate linear combination of outgoing two-body GSF, one in each coordinate \mathbf{r}_1 and \mathbf{r}_2 , and may be written as:

$$\Psi_{sc}^+(\mathbf{r}_1, \mathbf{r}_2) = \sum_{LM} \sum_{l_1 l_2} \sum_{n_1} \sum_{n_2} a_{n_1 n_2}^{LM l_1 l_2} \mathcal{A} \frac{S_{n_1 l_1}^+(r_1)}{r_1} \frac{S_{n_2 l_2}^+(r_2)}{r_2} \mathcal{Y}_{l_1 l_2}^{LM}(\hat{\mathbf{r}}_1, \hat{\mathbf{r}}_2). \quad (54)$$

Alternatively, one may use hyperspherical coordinates (see Section 4.5) $\rho = \sqrt{r_1^2 + r_2^2}$ and $\omega_5 = \{\alpha, \hat{\mathbf{r}}_1, \hat{\mathbf{r}}_2\}$, with $\alpha = \tan^{-1}(r_2/r_1)$, and write

$$\Psi_{sc}^+(\mathbf{r}_1, \mathbf{r}_2) = \sum_{mv} \tilde{a}_{mv} \frac{S_{mv}^+(\rho)}{\rho^{5/2}} \Omega_\nu(\omega_5). \quad (55)$$

Above, outgoing behavior (+) was chosen for the scattering states, $a_{n_1 n_2}^{LM l_1 l_2}$ and \tilde{a}_{mv} are linear coefficients, and the label ν collects all angular quantum numbers and summation indexes.

Other approaches for atoms and molecules based on Sturmian functions can be found in the literature. In the work of Piraux and collaborators, CSF are used to study different ionization processes produced by photon absorption and electron impact on atoms.^{9,10,11} CSF have been also used by Papp and collaborators^{69,70} to deal with three-body problem involving Coulomb plus short-range interactions within a Faddeev approach. Regarding issues of interest in quantum chemistry as applied to the electronic structure of atoms and molecules, Coulomb Sturmians pertaining to coordinate systems alternative to the spherical ones have also been developed and tested numerically for three-body problems.^{20,23} A different line has been implemented by Ovchinnikov.³¹ However, all these approaches are very different to the one reviewed here.

4.2 Asymptotic behaviors

To illustrate the different three-body asymptotic channels, consider the collision of an electron with hydrogen. Depending on the energy of the projectile, one or more processes may occur, in particular elastic scattering, scattering with simultaneous excitation of the residual target, or ionization

with two electrons escaping in the field of a proton. The three-body wave function solving the electron–hydrogen Schrödinger equation must contain simultaneously—i.e., it couples—all these possible processes. When solving the differential equation two major difficulties appear: (i) numerically expensive large grids are required since scattering states are spread and the probability of finding the particles at any point of the configuration space is different from zero; and (ii) it is far from obvious to impose as boundary conditions the well-defined asymptotic behaviors in different spacial domains.

Consider first the Ω_0 region, the one corresponding to all three particles far from each other. As all interparticle distances are large, no contributions coming from bound states are expected in the asymptotic three-body scattering wave function. Various approximated solutions are known for this region.^{72–74,76–78} An hyperspherical wave is known to be also a correct solution⁸:

$$\Psi_{as,c}^+(\mathbf{r}_1, \mathbf{r}_2) \xrightarrow{\rho \rightarrow \infty} \frac{(2\pi i)^{1/2}}{(2\pi)^3} K^{3/2} T_{\tilde{\mathbf{k}}_1, \tilde{\mathbf{k}}_2} \frac{e^{iK\rho - i\lambda_0 \ln(2K\rho) - i\sigma_0}}{\rho^{5/2}}, \quad (56)$$

where λ_0 is a Coulomb parameter, σ_0 is a phase and $T_{\tilde{\mathbf{k}}_1, \tilde{\mathbf{k}}_2} = T\left(\frac{K}{\rho}\mathbf{r}_1, \frac{K}{\rho}\mathbf{r}_2\right)$ is the ionization transition amplitude. The coordinate-dependent momenta $\tilde{\mathbf{k}}_j$ ($j = 2, 3$) were defined originally by Alt and Mukhamedzhanov,⁷⁴ while $K = \sqrt{k_1^2 + k_2^2}$ is the hyper-momentum of the particles.

Next, take the Ω_i regions (with $i = 1, 2, 3$) which correspond to two of the particles close to each other and the third is far away from the pair.⁷⁵ We may have the situation in which one of the electrons is close to the nucleus, forming a bound state, and the other is far away. In this case, the wave function should have the following asymptotic form:

$$\Psi_{as,1}^+(\mathbf{r}_1, \mathbf{r}_2) \xrightarrow{r_1 \rightarrow \infty} \Psi_i(\mathbf{r}_1, \mathbf{r}_2) - \frac{1}{2\pi} \sum_n^{\hat{f}} F_n(k_n \hat{\mathbf{r}}_1, \mathbf{k}_i) \frac{e^{ik_n r_1 - i\eta_1 \ln(2k_n r_1)}}{r_1} \phi_n(\mathbf{r}_2), \quad (57)$$

where $\Psi_i(\mathbf{r}_1, \mathbf{r}_2)$ represents the initial state which is defined before the collision. Here we are assuming that electron 1 is the projectile and η_1 is the corresponding Sommerfeld parameter. The second term in this expression represents the excitation of the target and the dispersion of the projectile; $F_n(k_n \hat{\mathbf{r}}_1, \mathbf{k}_i)$ represents the excitation amplitude. The symmetric case is the situation where the other electron is far away and the initial one ends up bound at the target

$$\Psi_{as,2}^+(\mathbf{r}_1, \mathbf{r}_2) \xrightarrow{r_2 \rightarrow \infty} -\frac{1}{2\pi} \sum_m \int G_m(k_m \hat{\mathbf{r}}_2, \mathbf{k}_i) \frac{e^{ik_m r_2 - i\eta_2 \ln(2k_m r_2)}}{r_2} \phi_m(\mathbf{r}_1), \quad (58)$$

where $G_m(k_m \hat{\mathbf{r}}_2, \mathbf{k}_i)$ represents the capture of the incoming electron and η_2 the Sommerfeld parameter for electron 2. The summations in Eq. (57) and (58) run over bound and continuum states. The third Ω_i region corresponds to the situation where both electrons are close to each other and far away from the nucleus.

When the collision process is studied and the Schrödinger equation is solved numerically, all the channels, represented by the asymptotic wave functions $\Psi_{as,1}^+(\mathbf{r}_1, \mathbf{r}_2)$, $\Psi_{as,2}^+(\mathbf{r}_1, \mathbf{r}_2)$, and $\Psi_{as,c}^+(\mathbf{r}_1, \mathbf{r}_2)$, are coupled and are incorporated simultaneously into the solution. In other words, the full solution should have the following general form at large distances:

$$\Psi^+(\mathbf{r}_1, \mathbf{r}_2) \xrightarrow{\rho \rightarrow \infty} \Psi_{as,1}^+(\mathbf{r}_1, \mathbf{r}_2) + \Psi_{as,2}^+(\mathbf{r}_1, \mathbf{r}_2) + \Psi_{as,c}^+(\mathbf{r}_1, \mathbf{r}_2). \quad (59)$$

Numerically, it is extremely difficult to impose these conditions to the wave function. As mentioned in the introduction, however, various methods have succeeded but not without difficulties. In this section, we shall see how GSF can be used to tackle the problem. Applications for several processes will be given in Section 5.

4.3 Driven equation for three-body scattering problems

A standard procedure to solve three-body scattering problems consists in transforming the homogeneous three-body Schrödinger equation into an inhomogeneous one (driven equation). As in Section 2.3, Eq. (21), the three-body solution is separated as the sum of an initial channel wave function $\Psi_i(\mathbf{r}_1, \mathbf{r}_2)$ and the scattering wave function $\Psi_{sc}^+(\mathbf{r}_1, \mathbf{r}_2)$ which contains all the information about the collision process:

$$\Psi^+(\mathbf{r}_1, \mathbf{r}_2) = \Psi_i(\mathbf{r}_1, \mathbf{r}_2) + \Psi_{sc}^+(\mathbf{r}_1, \mathbf{r}_2). \quad (60)$$

When this proposal is substituted into the Schrödinger equation (40) the following driven equation results for $\Psi_{sc}^+(\mathbf{r}_1, \mathbf{r}_2)$

$$[H - E] \Psi_{sc}^+(\mathbf{r}_1, \mathbf{r}_2) = -W(\mathbf{r}_1, \mathbf{r}_2) \Psi_i(\mathbf{r}_1, \mathbf{r}_2), \quad (61)$$

where $W(\mathbf{r}_1, \mathbf{r}_2)$ represents the interactions not solved by $\Psi_i(\mathbf{r}_1, \mathbf{r}_2)$.

It is interesting to notice that the transition amplitude $T_{\tilde{\mathbf{k}}_1, \tilde{\mathbf{k}}_2}^-$ appearing in Eq. (56) can be extracted directly from the solution of (61) which, formally, may be written as:

$$\Psi_{sc}^+(\mathbf{r}_1, \mathbf{r}_2) = \int d\mathbf{r}'_1 d\mathbf{r}'_2 G^+(\mathbf{r}_1, \mathbf{r}_2, \mathbf{r}'_1, \mathbf{r}'_2) W(\mathbf{r}'_1, \mathbf{r}'_2) \Psi_i(\mathbf{r}'_1, \mathbf{r}'_2), \quad (62)$$

where $G^+(\mathbf{r}_1, \mathbf{r}_2, \mathbf{r}'_1, \mathbf{r}'_2)$ is the three-body Coulomb Green's function. In the Ω_0 region its asymptotic limit reads⁸

$$G^+(\mathbf{r}_1, \mathbf{r}_2, \mathbf{r}'_1, \mathbf{r}'_2) \rightarrow \frac{(2\pi i)^{1/2}}{(2\pi)^3} K^{\frac{3}{2}} \frac{e^{i[K\rho - \lambda_0 \ln(2K\rho) - \sigma_0]}}{\rho^{\frac{5}{2}}} \Psi_{\tilde{\mathbf{k}}_1, \tilde{\mathbf{k}}_2}^-(\mathbf{r}'_1, \mathbf{r}'_2), \quad (63)$$

where the function $\Psi_{\tilde{\mathbf{k}}_1, \tilde{\mathbf{k}}_2}^-(\mathbf{r}'_1, \mathbf{r}'_2)$ is the exact solution of the three-body problem with incoming wave asymptotic behavior.

From these two relations, one finds that the scattering wave function $\Psi_{\mathbf{k}_1, \mathbf{k}_2}^-(\mathbf{r}'_1, \mathbf{r}'_2)$ will have the asymptotic behaviour (56) in which the transition amplitude $T_{\tilde{\mathbf{k}}_1, \tilde{\mathbf{k}}_2}^-$ is given by

$$T_{\tilde{\mathbf{k}}_1, \tilde{\mathbf{k}}_2}^- = \langle \Psi_{\tilde{\mathbf{k}}_1, \tilde{\mathbf{k}}_2}^-(\mathbf{r}_1, \mathbf{r}_2) | W(\mathbf{r}_1, \mathbf{r}_2) | \Psi_i(\mathbf{r}_1, \mathbf{r}_2) \rangle. \quad (64)$$

This is the standard definition for the transition amplitudes required by scattering theory. Thus, once the driven Eq. (61) is solved with appropriate asymptotic conditions, one can extract the ionization transition amplitude from the evaluation—at large distances—of the scattering wave function itself. However, since all possible channels are coupled, it is possible to extract also the other transition amplitudes appearing in Eqs. (57) and (58).

4.3.1 Ionization of hydrogen by electron impact

In the case of an electron-hydrogen collision, the Hamiltonian H is given by Eq. (50) where $z_1 = z_2 = -1$ and $z_3 = Z = 1$. The initial state may

be chosen as a plane wave for the incident electron $e^{i\mathbf{k}_i \cdot \mathbf{r}_1}$ multiplied by an hydrogenic ground state e^{-Zr_2} ; actually, depending whether one looks at singlet ($S = 0$) or triplet ($S = 1$) states, one may take the following combination

$$\Psi_i(\mathbf{r}_1, \mathbf{r}_2) = \mathcal{A} \frac{1}{\sqrt{\pi}} e^{-r_1} e^{i\mathbf{k}_i \cdot \mathbf{r}_2},$$

where $k_i = \sqrt{2(E - (-Z^2/2))}$. The RHS of the driven equation (61) is then

$$- \left[\left(\frac{1}{r_{12}} - \frac{1}{r_2} \right) \Psi_i(\mathbf{r}_1, \mathbf{r}_2) + (-1)^S (1 \leftrightarrow 2) \right]. \quad (65)$$

Other proposals including correlation can be defined for the initial state. For example, a C3-like approach where the projectile–target interaction is explicitly included presents the advantage of leading to a short-range $W(\mathbf{r}_1, \mathbf{r}_2)$ function.⁷⁹ However, it has the disadvantage of coupling all the coordinates and making more difficult the task of solving the driven equation.

4.3.2 Double ionization of helium by high-energy electron impact

Consider now the double ionization of helium atoms by high-energy electron impact. As shown in Ref. 80 and briefly sketched below, this four-body scattering problem can be reduced to a three-body problem, and thus we end up with a driven equation of the kind (61).

The non-relativistic four-body Hamiltonian for three electrons and an infinite mass helium nucleus of charge $Z = 2$ is given by

$$H_{4b} = -\frac{1}{2}\nabla_0^2 - \frac{1}{2}\nabla_1^2 - \frac{1}{2}\nabla_2^2 - \frac{Z}{r_0} - \frac{Z}{r_1} - \frac{Z}{r_2} + \frac{1}{r_{01}} + \frac{1}{r_{02}} + \frac{1}{r_{12}}, \quad (66)$$

where particle 0 labels the electron projectile (incident with momentum \mathbf{k}_i , and scattered with momentum \mathbf{k}_f), while particles 1 and 2 are the target electrons. We first define a projectile Hamiltonian

$$H_p(Z_p) = \left(-\frac{1}{2}\nabla_0^2 - \frac{Z_p}{r_0} \right), \quad (67)$$

which includes only Coulomb projectile–nucleus interaction with a model charge Z_p . We then decompose the four-body Hamiltonian as follows:

$$H_{4b} = H_0 (Z_p) + \bar{W} (Z_p), \quad (68)$$

where

$$H_0 (Z_p) = H_p(Z_p) + H_a, \quad (69a)$$

$$\bar{W} (Z_p) = -\frac{Z - Z_p}{r_0} + \frac{1}{r_{01}} + \frac{1}{r_{02}}. \quad (69b)$$

Above H_a is the three-body helium Hamiltonian (50); let $\Phi^{(0)}(\mathbf{r}_1, \mathbf{r}_2)$ represent its ground state. As well as all kinetic operators, the Hamiltonian $H_0 (Z_p)$ includes all interactions of the subsystem (1,2) through H_a , and a projectile–nucleus interaction $-Z_p/r_0$ through $H_p(Z_p)$. The two subsystems are coupled through the interaction $\bar{W}(Z_p)$ which may be considered as a perturbation.

To study electron-impact double ionization processes we need to find a scattering solution, with outgoing-type behavior, of the four-body Schrödinger equation

$$[H_0 (Z_p) + \bar{W} (Z_p) - E] \Psi^+ (\mathbf{r}_0, \mathbf{r}_1, \mathbf{r}_2) = 0. \quad (70)$$

Using a perturbation expansion in terms of the magnitude of $\bar{W} (Z_p)$, $\Psi^+ = \sum_n \lambda^n \Psi^{(n)+}$, we obtain a system of differential equations for $\Psi^{(n)+}$. The function

$$\Psi^{(0)+} (\mathbf{r}_0, \mathbf{r}_1, \mathbf{r}_2) = \frac{1}{(2\pi)^{3/2}} e^{i\mathbf{k}_i \cdot \mathbf{r}_0} \Phi^{(0)} (\mathbf{r}_1, \mathbf{r}_2), \quad (71)$$

solution of the Hamiltonian H_0 (which is separable in the two subsystems (1,2) and 0), represents the initial state of the system (zeroth-order equation). For presentation purposes, the projectile–nucleus interaction is neglected and a plane wave is taken ($Z_p = 0$). Alternatively (see Ref. 80, for details), it can be properly represented through a Coulomb wave function with charge $Z_p = Z^{81}$ which includes the projectile–nucleus interaction in both initial and final channels.

Next, we explore the first-order equation in which the interaction $\bar{W}(Z_p)$ is included only once. Taking a plane wave for the scattered electron, the two ejected electrons solution satisfies the driven equation⁸⁰

$$[E_a - H_a] \Phi_{sc}^{(1)+}(\mathbf{r}_1, \mathbf{r}_2) = W_{fi}(\mathbf{r}_1, \mathbf{r}_2) \Phi^{(0)}(\mathbf{r}_1, \mathbf{r}_2), \quad (72)$$

where $E_a = E - k_f^2/2$ denotes the energy of two electrons in interaction with the nucleus in the final state, and the driven term includes

$$W_{fi}(\mathbf{r}_1, \mathbf{r}_2) = \langle \mathbf{k}_f | \bar{W} | \mathbf{k}_i \rangle = \frac{1}{(2\pi)^3} \frac{4\pi}{q^2} \left(-Z + e^{i\mathbf{q}\cdot\mathbf{r}_1} + e^{i\mathbf{q}\cdot\mathbf{r}_2} \right) \quad (73)$$

with $\mathbf{q} = \mathbf{k}_i - \mathbf{k}_f$ the momentum transfer. In this way, the four-body problem is reduced to a pure three-body one as described by (61) where the dynamics of the two ejected electrons in the presence of the heavy nucleus is described by Eq. (72). The four-body scattering problem is well formulated and its first-order solution possesses all the information contained in the first Born approximation. Following similar steps used for the three-body case, we can extract a transition amplitude (64) that in this case reads

$$T_{\tilde{\mathbf{k}}_1, \tilde{\mathbf{k}}_2} = \frac{1}{(2\pi)^3} \frac{4\pi}{q^2} \langle \Psi_{\tilde{\mathbf{k}}_1, \tilde{\mathbf{k}}_2}^- (\mathbf{r}_1, \mathbf{r}_2) | -Z + e^{i\mathbf{q}\cdot\mathbf{r}_1} + e^{i\mathbf{q}\cdot\mathbf{r}_2} | \Phi^{(0)}(\mathbf{r}_1, \mathbf{r}_2) \rangle \quad (74)$$

and one recovers the standard first Born approximation, see, e.g., Ref. 82,83. In the calculations presented in the literature, approximated wave functions, or numerical ones, have been used for $\Psi_{\tilde{\mathbf{k}}_1, \tilde{\mathbf{k}}_2}^- (\mathbf{r}_1, \mathbf{r}_2)$. In the transition matrix element (74) the exact solution of the three-body problem $\Psi_{\tilde{\mathbf{k}}_1, \tilde{\mathbf{k}}_2}^- (\mathbf{r}_1, \mathbf{r}_2)$ should be used; the corresponding three-body Schrödinger equation has been given, for the first time, in Ref. 80.

Whether for single ionization of hydrogen, or double ionization of helium by fast incident electrons, the scattering problem is transformed into a three-body driven equation (Eq. (61) or (72)) with outgoing boundary conditions. These equations can be solved with GSF either in spherical or hyperspherical coordinates.

4.4 Solving the driven equation with GSF (spherical coordinates)

In order to solve the driven equation (61), we may use a *CI* expansion (54). Projecting over the basis elements a matrix problem results,

$$[\mathbf{S}(E - E_1 - E_2) - \mathbf{H}] \mathbf{a} = \mathbf{b}, \tag{75}$$

where the Hamiltonian \mathbf{H} and overlap \mathbf{S} matrices have elements $[\mathbf{H}]_{n'_1 n'_2 n_1 n_2}^{l'_1 l'_2 l_1 l_2}$ and $[\mathbf{S}]_{n'_1 n'_2 n_1 n_2}^{l'_1 l'_2 l_1 l_2}$ similar to those described for the three-body bound states, except that the GSF have outgoing behavior.

The elements of the vector \mathbf{b} are the expansion coefficients of the driven term

$$W(\mathbf{r}_1, \mathbf{r}_2) \Psi_i(\mathbf{r}_1, \mathbf{r}_2) = \sum_{LMl_1 l_2} \sum_{n_1} \sum_{n_2} b_{n_1 n_2}^{LMl_1 l_2} \mathcal{V}_{g_1}(r_1) \mathcal{V}_{g_2}(r_2) \mathcal{A} \left(\frac{S_{n_1 l_1}^+(r_1)}{r_1} \frac{S_{n_2 l_2}^+(r_2)}{r_2} \mathcal{Y}_{l_1 l_2}^{LM}(\hat{\mathbf{r}}_1, \hat{\mathbf{r}}_2) \right). \tag{76}$$

Note that, using the generating potentials $\mathcal{V}_{g_1}(r_1)$ and $\mathcal{V}_{g_2}(r_2)$, the orthogonality property of the GSF makes the matrices diagonal and leads to a largely simplified calculation. One of the advantages of using the GSF is that they remove from the equation the kinetic energy of each electron, and the electron–nucleus potentials by taking them as auxiliary potentials in Eq. (2). In this way, only the generating potentials and the electron–electron interaction have to be evaluated to obtain Hamiltonian \mathbf{H} .

4.5 Solving the driven equation with GSF (hyperspherical coordinates)

We shall now present an hyperspherical approach. To do so, we first need to define the coordinates, set the scattering problem, and then propose hyperspherical GSF to solve it.

4.5.1 Hyperspherical coordinates

The three-body Hamiltonian with particles of masses m_1, m_2 , and m_3 can be written in terms of mass-scaled Jacobi coordinates \mathbf{x} and \mathbf{X} .^{21,22,84,85} From these vectors, which represent any of the three existing pairs in three-body problems, hyperspherical coordinates can be defined: a hyperradius ρ , defined as $\rho^2 = x^2 + X^2$, and five hyperangular coordinates (denoted collectively by ω_5) that include the hyperangle $\tan \alpha = X/x$ and the polar angles θ_x, ϕ_x and θ_X, ϕ_X defining the orientations $\hat{\mathbf{x}}$ and $\hat{\mathbf{X}}$ of the Jacobi vectors in the center-of-mass reference frame. The previous definitions allow one to write $x = \rho \cos \alpha$ and $X = \rho \sin \alpha$; below $x = r_1$ and $X = r_2$.

The three-body Hamiltonian is now written as $H = T + V(\rho, \omega_5)$ where the kinetic energy operator takes the form

$$T = -\frac{1}{2\mu} \left[\frac{1}{\rho^5} \frac{\partial}{\partial \rho} \left(\rho^5 \frac{\partial}{\partial \rho} \right) - \frac{\Lambda^2}{\rho^2} \right],$$

where $\mu = \sqrt{m_1 m_2 m_3 / (m_1 + m_2 + m_3)}$ is the three-body reduced mass, and Λ^2 is the grand orbital angular momentum operator.⁸⁴

The interaction potentials, say between two electrons (positions $\mathbf{r}_1, \mathbf{r}_2$) and a nucleus of charge Z , may be written as^{86,30}

$$V(\rho, \omega_5) = -\frac{Z}{r_1} - \frac{Z}{r_2} + \frac{1}{r_{12}} = \frac{C(\omega_5)}{\rho}, \quad (77)$$

where

$$C(\omega_5) = -\frac{Z}{\cos \alpha} - \frac{Z}{\sin \alpha} + \sum_{l=0}^{\infty} \frac{4\pi}{2l+1} \times \sum_{m=-l}^l (-1)^m Y_{l-m}(\hat{\mathbf{r}}_2) Y_{lm}(\hat{\mathbf{r}}_1) \left\{ \begin{array}{l} \sec \alpha \tan^l \alpha \\ \csc \alpha \cot^l \alpha \end{array} \right\}, \quad (78)$$

the top choice (between brackets) being for $0 \leq \alpha \leq \frac{1}{4}\pi$ and the bottom one for $\frac{1}{4}\pi \leq \alpha \leq \frac{1}{2}\pi$.

4.5.2 Scattering driven equation

The Schrödinger equation to be considered is $[H - E] \Psi(\rho, \omega_5) = 0$. As proposed in spherical coordinates (see Eq. (60)), the wave function $\Psi(\rho, \omega_5)$ for a collision process may be separated in two parts $\Psi(\rho, \omega_5) = \Psi_i(\rho, \omega_5) + \Psi_{sc}(\rho, \omega_5)$. Again, $\Psi_i(\rho, \omega_5)$ is a known initial state, eigensolution of an approximate Hamiltonian $H_0 = H - W$. Recall that since $H = T + V(\rho, \omega_5)$ is the full Hamiltonian, W is the neglected, unsolved interaction not included in the initial prepared state. $\Psi_{sc}(\rho, \omega_5)$, on the other hand, is a wave function solving all the interactions $V(\rho, \omega_5)$. According to this separation, the function $\Psi_{sc}(\rho, \omega_5)$ satisfies a driven Schrödinger equation

$$[T + V(\rho, \omega_5) - E] \Psi_{sc}(\rho, \omega_5) = -W(\rho, \omega_5) \Psi_i(\rho, \omega_5) = \varphi(\rho, \omega_5), \quad (79)$$

where $\varphi(\rho, \omega_5)$ denotes the driving term. Equation (79) must be solved imposing outgoing behavior to $\Psi_{sc}(\rho, \omega_5)$ for large values of ρ ($\rho \rightarrow \infty$).

Let K be the hyperspherical momentum related to the total energy through $E = K^2/2\mu$. When all particles are far from each other, the Peterkop-type asymptotic behavior

$$\Psi_{sc}^+(\rho, \omega_5) \propto \frac{e^{iK\rho - i\frac{C(\omega_5)}{K} \ln(2K\rho)}}{\rho^{5/2}} \quad (80)$$

indicates that an hyperspherical approach could be more adequate than the use of interparticle (spherical) coordinates. It also shows that, in the asymptotic region, the Coulomb interactions couple the angles with the hyperradius in a particular form, through a Coulomb logarithmic phase.

Two important issues when solving this collision problem are (i) the range of the interaction $W(\rho, \omega_5)$ and (ii) the use of an appropriate matrix definition for the operator $(H - E)$ or for Green's function $(H - E)^{-1}$. The basis set to be used has to take into account both issues: it has to be complete in the region where the interaction $W(\rho, \omega_5)$ is not negligible, and outside that region has to possess the correct asymptotic behavior corresponding to all three Coulomb interactions.

4.5.3 Hyperspherical Generalized Sturmian functions

There are various ways of defining a Sturmian strategy in hyperspherical coordinates. Two of them were discussed in Refs. 84,86. Here we briefly review the approach presented in Ref. 84.

First, as in Ref. 30, we define a set of angular Sturmian functions $\Omega_\nu(\omega_5)$ depending on the angular coordinates ω_5 . They are solutions of the following angular Sturmian eigenvalue equation

$$\left[\Lambda^2 + 2\mu\rho_\nu C(\omega_5) \right] \Omega_\nu(\omega_5) = \nu(\nu + 4)\Omega_\nu(\omega_5), \quad (81)$$

where ρ_ν or, alternatively, ν can be considered as the eigenvalues. If ν is used as eigenvalue, then ρ_ν is considered as an externally fixed parameter ρ_{eff} (there are various ways of defining ρ_{eff} , some of them have been discussed in Ref. 84). In this case, the eigenfunctions $\Omega_\nu(\omega_5)$ satisfy the following orthogonality and closure relations

$$\int d\omega_5 \Omega_{\nu'}(\omega_5) \Omega_\nu(\omega_5) = \delta_{\nu'\nu}, \quad (82a)$$

$$\sum_{\nu} \Omega_{\nu}(\omega'_5) \Omega_{\nu}(\omega_5) = \delta(\omega_5 - \omega'_5), \quad (82b)$$

where $d\omega_5$ represents the five-dimensional volume element and $\delta(\omega_5 - \omega'_5)$ is the symbolic product of the Dirac delta corresponding to all five angular coordinates.

In the specific case of the S -wave models to be considered in the applications (Section 5), the eigenfunctions are the Jacobi polynomials^{21,22,84,86}

$$\Omega_n(\alpha) = \frac{4(n+1)}{\sqrt{\pi}} {}_2F_1\left(-n, n+2, \frac{3}{2}; \sin^2 \alpha\right), \quad (83)$$

where ${}_2F_1$ represents the Gauss hypergeometric function.⁸⁷ These angular functions satisfy the eigenvalue equation

$$\Lambda^2 \Omega_n(\alpha) = \nu_n(\nu_n + 4) \Omega_n(\alpha), \quad (84)$$

with $\nu_n = 2n$ ($n = 0, 1, \dots$), form a complete set and satisfy the orthonormality relation

$$\int_0^{\pi/2} \Omega_{n'}(\alpha) \Omega_n(\alpha) \sin^2 \alpha \cos^2 \alpha \, d\alpha = \delta_{n'n}. \quad (85)$$

For the hyperradial coordinate we can introduce a set of radial functions $\bar{S}_{m\nu}(\rho)$ satisfying the Sturmian equation:

$$\begin{aligned} & \left[-\frac{1}{2\mu} \frac{1}{\rho^5} \frac{\partial}{\partial \rho} \left(\rho^5 \frac{\partial}{\partial \rho} \right) + \frac{\nu(\nu+4)}{2\mu\rho^2} + \mathcal{U}(\rho) - E \right] \bar{S}_{m\nu}(\rho) \\ & = -\beta_m \mathcal{V}_g(\rho) \bar{S}_{m\nu}(\rho). \end{aligned} \quad (86)$$

The potential $\mathcal{U}(\rho)$ can be of short- or long-range; $\mathcal{V}_g(\rho)$ is a generating potential. Introducing the reduced function $\bar{S}_{m\nu}(\rho) = S_{m\nu}(\rho) / \rho^{\frac{5}{2}}$ into (86) leads to

$$\left[-\frac{1}{2\mu} \frac{\partial^2}{\partial \rho^2} + \frac{\nu(\nu+4) + \frac{15}{4}}{2\mu\rho^2} + \mathcal{U}(\rho) - E \right] S_{m\nu}(\rho) = -\beta_m \mathcal{V}_g(\rho) S_{m\nu}(\rho), \quad (87)$$

which has the same form as Eq. (2) presented in Section 2.1 (the difference appearing only in the definition of the $1/\rho^2$ term) and similar boundary conditions can then be used. Note that the parameter ν can be a fixed parameter or the eigenvalue of the angular Sturmian functions. The hyper-radial eigenfunctions $S_{m\nu}(\rho)$ form an orthogonal and complete set such that

$$\int d\rho S_{m'\nu}(\rho) \mathcal{V}_g(\rho) S_{m\nu}(\rho) = \delta_{m'm}, \quad (88a)$$

$$\sum_m S_{m\nu}(\rho') \mathcal{V}_g(\rho) S_{m\nu}(\rho) = \delta(\rho - \rho') \quad (88b)$$

and the algebra maps easily to the one related to the spherical radial Sturmian functions.

4.5.4 Hyperspherical Generalized Sturmian functions applied to scattering problems

To solve the driven Eq. (79), we use expansion (55) for the wave function $\Psi_{sc}(\rho, \omega_5)$. We also propose the following expansion for the driven term

$$W(\rho, \omega_5) \Psi_i(\rho, \omega_5) = \sum_{m\nu} c_{m\nu} \mathcal{V}_g(\rho) \frac{S_{m\nu}(\rho)}{\rho^{\frac{5}{2}}} \Omega_\nu(\omega_5), \quad (89)$$

whose range dictates that of the generating potential $\mathcal{V}_g(\rho)$ to be chosen. Replacing in (79) we obtain

$$\begin{aligned} \sum_{m\nu} \tilde{a}_{m\nu} \left[\left(\mathcal{U}(\rho) + \beta_m \mathcal{V}_g(\rho) \right) + \rho_{\text{eff}} \frac{C(\omega_5)}{\rho^2} + \frac{C(\omega_5)}{\rho} \right] S_{m\nu}(\rho) \Omega_\nu(\omega_5) \\ = W(\rho, \omega_5) \Psi_i(\rho, \omega_5), \end{aligned} \quad (90)$$

One convenient election for the potential $\mathcal{U}(\rho)$ could be $\mathcal{U}(\rho) = -Z/\rho$. Projecting Eq. (90) over the basis functions, and using the orthogonality properties (82a) and (88a), we find

$$\begin{aligned} \sum_{m\nu} \left[\left(\left[\frac{-Z}{\rho} \right]_{mm',\nu} + \beta_m \delta_{mm'} \right) \delta_{\nu\nu'} + \left(\rho_{\text{eff}} \left[\frac{1}{\rho^2} \right]_{mm',\nu} + \left[\frac{1}{\rho} \right]_{mm',\nu} \right) [C(\omega_5)]_{\nu\nu'} \right] \\ \tilde{a}_{m\nu} = c_{m'\nu'}, \end{aligned} \quad (91)$$

where the matrix elements $[C(\omega_5)]_{vv'}$ are

$$[C(\omega_5)]_{vv'} = \int d\omega_5 \Omega_{v'}(\omega_5) C(\omega_5) \Omega_v(\omega_5), \quad (92)$$

and the matrix elements $[A]_{mm',y}$ are defined by one-dimensional integrals

$$[A]_{mm',y} = \int d\rho S_{mv}(\rho) A(\rho) S_{m'v}(\rho). \quad (93)$$

Solving the matrix problem (91) provides the expansion coefficients \tilde{a}_{mv} . In the next section, we see that building the solution in this way provides the scattering functions with the correct asymptotic behavior (80).



5. THREE-BODY SCATTERING STATES: APPLICATIONS

5.1 Introduction

Model calculations, used as benchmarks, can be found throughout the collision literature. *S*-wave models, though restricted to zero angular momentum states, serve as a test bed as they contain most of the features and difficulties associated to the full physical problem but, require less computational resources. They are useful, in general, as they allow us to put on a strong footing different numerical methods which do not necessarily yield converging results when applied to complicated scattering processes. For the three-body problem, for example, before solving the full electron–Hydrogen ionization problem, *S*-wave model (often referred to as Temkin–Poet (TP) model^{88,89}) calculations have played a very important role in the development of theoretical methods.

In this section we consider three-body scattering *S*-wave models solved using GSF. We start with a recently proposed break-up model problem, then consider the electron–Hydrogen TP model (*e*, 2*e*) processes, and finally a model calculation for high impact energy (*e*, 3*e*) processes.

In the TP model, the electron–electron repulsion $1/r_{12}$ is spherically averaged and thus replaced by $1/r_>$ where $r_> = \max(r_1, r_2)$. The three-body Coulomb potential (two electrons and a nucleus of charge *Z*) becomes

$$V(r_1, r_2) = -\frac{Z}{r_1} - \frac{Z}{r_2} + \frac{1}{r_>}. \quad (94)$$

In hyperspherical coordinates, the “charge” $C(\omega_5)$ defined through (77) is replaced by $\tilde{C}(\alpha)$ with

Thus only an α dependence is retained in the potential: $V(\rho, \omega_5) = \tilde{C}(\alpha)/\rho$.

$$\tilde{C}(\alpha) = -\frac{Z}{\cos \alpha} - \frac{Z}{\sin \alpha} + \begin{cases} \frac{1}{\cos \alpha} & 0 \leq \alpha \leq \frac{1}{4}\pi \\ \frac{1}{\sin \alpha} & \frac{1}{4}\pi \leq \alpha \leq \frac{1}{2}\pi. \end{cases} \quad (95)$$

The Schrödinger equation corresponding to the TP model provides a simplified version of the physical problem.

5.2 Three-body S-wave model problem

Recently,⁹⁰ a three-body S-wave model has been proposed. Though apparently rather simple, this model contains the essential difficulties of the real problem (Coulomb potentials and non-separability). As the analytical solution of the model can be written out, it provides a very interesting and unique tool to validate numerical methods.

Differently from the TP model, the authors of Ref. 90 suggested replacing $C(\omega_5)$ by a constant charge \mathcal{C} , i.e., the following model Coulomb potential

$$V(\rho) = \frac{\mathcal{C}}{\rho}, \quad (96)$$

which can be either attractive ($\mathcal{C} < 0$) or repulsive ($\mathcal{C} > 0$). Note that the potential is not one of the three Coulomb interactions that appear in the physical case $V(\rho, \omega_5)$. Although seemingly simple in hyperspherical coordinates, it is not separable in spherical coordinates r_1 and r_2 ; assuming, for example, that $r_2 < r_1$, their coupling is very particular

$$\frac{\mathcal{C}}{\sqrt{r_1^2 + r_2^2}} = \frac{\mathcal{C}}{r_1} \left[1 - \frac{1}{2} \left(\frac{r_2}{r_1} \right)^2 + \dots \right] = \frac{\mathcal{C}}{\rho \cos \alpha} \left[1 - \frac{1}{2} \tan^2 \alpha + \dots \right], \quad (97)$$

where the second equality illustrates the expansion in terms of the hyper-angle α . The lowest order (first term) of expansion (97) corresponds to retaining the first term of the real potential (77). The model potential (96) therefore tests the r_1 and r_2 dependence in a way which differs substantially from the TP model. On top of that, it offers the possibility to make a detailed and interesting asymptotic investigation of the scattering wave

function. Indeed, for a given “angular” set (fixed ω_5), the angular dependent charge $C(\omega_5)$ takes a constant value and thus the physical three-body potential reduces to the model. The knowledge of the analytic solution allows one to investigate, in an original manner, for what hyperradius the corresponding asymptotic regime is actually reached. By varying the angles, one may explore different asymptotic domains, and related convergence issues.

In the proposed model, the initial state is taken to be a symmetrized bound-free product of a standing spherical wave in the relative coordinate r_1 between the incoming particle and the center of the target and a bound-like state in the target coordinate r_2 ; the interaction neglected in the initial channel is given, for example, by a Yukawa potential $e^{-a\rho}/\rho$. More specifically, we take the following source (driving term)

$$\varphi(\rho, \alpha) = \rho^t e^{-a\rho} \frac{1}{2} \left[\frac{\sin r_1 \sinh r_2}{r_1 r_2} + \frac{\sin r_2 \sinh r_1}{r_2 r_1} \right], \quad (98)$$

with a parameter a such that $\Re(a) > 1$ and a real parameter $t \geq -1$. This source has a known single series expansion in Jacobi polynomials $\Omega_n(\alpha)$, the coefficients being functions of ρ .

The Coulomb potential is simple in hyperspherical but not in spherical coordinates. The driven term is not separable in either set of coordinates, not even asymptotically. Thus the model equation

$$\left[-\frac{1}{2\mu} \frac{1}{\rho^5} \frac{\partial}{\partial \rho} \left(\rho^5 \frac{\partial}{\partial \rho} \right) + \frac{\Lambda^2}{2\mu\rho^2} + \frac{\mathcal{C}}{\rho} - E \right] \Psi(\rho, \alpha) = \varphi(\rho, \alpha), \quad (99)$$

together with the source (98) provides a physically meaningful Coulomb scattering problem which presents typical three-body problem difficulties including non-separability.

To numerically solve this three-body problem hyperspherical Sturmian functions, built as a product of coupled functions (55), were employed.^{90,91} For the angular part, Jacobi polynomials $\Omega_n(\alpha)$ were used and can be generated either through their analytic definition (83) or by solving numerically the hyperangular eigenvalue equation (84) by discretizing the functions on a uniform angular lattice.⁹¹ Within a finite-difference scheme and using a second-order approximation, a discretized version of this equation is obtained and solved efficiently using standard matrix diagonalization

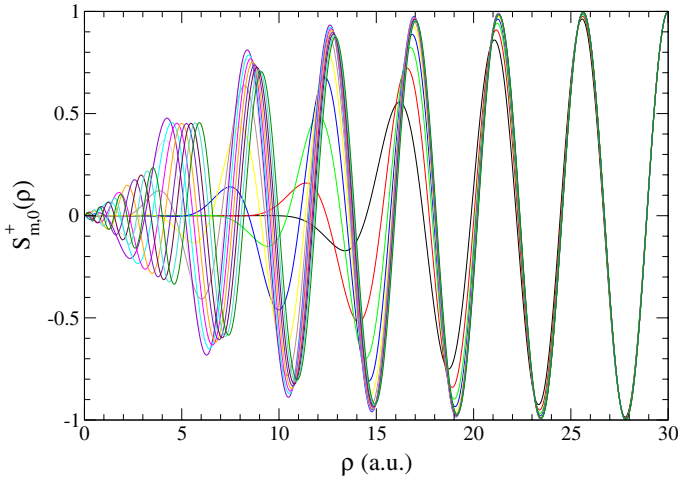


Figure 7.6 The first 15 Generalized Hyperspherical Sturmian basis set $S_{mn}^+(\rho)$, for $n = 0$ and $E = 1$ a.u. For color version of this figure, the reader is referred to the online version of this chapter.

routines, such as those from Lapack package.⁹² Coupled to these angular functions, for a given n , we take as hyperradial basis functions, the Sturmian functions $S_{mn}(\rho)$ solving numerically Eq. (87) where $\nu = \nu_n = 2n$ and E is externally fixed as the energy of the system. The auxiliary potential $\mathcal{U}(\rho)$ is taken to be equal to the interaction potential \mathcal{C}/ρ , while the generating potential $\mathcal{V}_g(\rho)$ is set as a Yukawa potential $-\exp(-a_s\rho)/\rho$. With this choice, asymptotically, Eq. (87) reduces to a Coulomb homogeneous equation providing all basis functions (and thus the hyperspherical GSF) a unique—and appropriate—asymptotic behavior

$$\lim_{\rho \rightarrow \infty} S_{mn}^+(\rho) \propto e^{iK\rho - i\eta \ln(2K\rho)}, \quad (100)$$

where K is the hyperspherical momentum and $\eta = \mathcal{C}\mu/K$ the Sommerfeld parameter.

In Figure 7.6, the functions $S_{mn}^+(\rho)$, corresponding to the first 15 hyper-radial quantum numbers m , and for the hyperangular quantum number $n = 0$, obtained with $a_s = 0.2$, are plotted for a model attractive charge $\mathcal{C} = -1$, assuming a reduced mass $\mu = 1$, and for an energy $E = 1$ a.u. One easily appreciates how every function in the set achieves the asymptotic behavior (100) smoothly and the set is dense for low hyperradial values. Therefore, any well-behaved function that vanishes at $\rho < 25$ a.u., can be

perfectly expanded by this basis. For higher n values, the basis is dense for higher ρ values, allowing the expansion at a more extended range.

Let us expand the numerical solution of the scattering problem (99) with such a basis set

$$\Psi^{NUM}(\rho, \alpha) = \frac{1}{\rho^{\frac{5}{2}}} \sum_m \sum_n a_{mn} S_{mn}^+(\rho) \Omega_n(\alpha). \quad (101)$$

Since both $\Psi^{NUM}(\rho, \alpha)$ and $S_{mn}^+(\rho)$ have the same asymptotic behavior, the above expansion is restricted to the internal region where particle interaction occurs. Using the eigenvalue Eq. (84) for the angular part, Eq. (87) for the radial part, projecting over $S_{pq}^+(\rho)\Omega_q(\alpha)/\rho^{\frac{5}{2}}$ and using the orthonormality relation (85), the unknown coefficients a are given by the following matrix equation

$$\sum_m \beta_{p,m} [\mathbf{V}]_{p,qm} a_{pm} = I_{pq}, \quad (102)$$

where the matrix elements are defined as

$$[\mathbf{V}]_{p,qm} = \int_0^\infty S_{pq}^+(\rho) \mathcal{V}_g(\rho) S_{mq}^+(\rho) d\rho. \quad (103)$$

The RHS vector I_{pq} elements are defined by

$$I_{pq} = \int_0^{\pi/2} \Omega_p(\alpha) \sin^2 \alpha \cos^2 \alpha d\alpha \int_0^\infty S_{pq}^+(\rho) \varphi(\rho, \alpha) \rho^{\frac{5}{2}} d\rho, \quad (104)$$

which, for the source (98) considered, reduce to the product of one-dimensional integrals. The driven equation (99) is transformed into an algebraic problem which can be easily solved using standard matrix techniques.⁴³

The general solution of the complete scattering problem is known analytically.⁹⁰ It is built as a linear combination of products of hyperangular $\Omega_n(\alpha)$ functions times hyperradial functions^{90,93} built to have the desired outgoing asymptotic behavior

$$\Psi^+(\rho, \alpha) \rightarrow f(\alpha) \frac{e^{iK\rho - i\eta \ln(2K\rho)}}{\rho^{\frac{5}{2}}}, \quad (105)$$

expected for a Coulomb scattering problem.^{94,95} This limit provides an analytical expression also for the transition amplitude $f(\alpha)$. The latter can be easily extracted also from $\Psi^{NUM}(\rho, \alpha)$ using the outgoing asymptotic behavior (100), since

$$\Psi^{NUM}(\rho, \alpha) \rightarrow \sum_n \left(\sum_m a_{n,m} \right) \Omega_n(\alpha) \frac{e^{iK\rho - i\eta \ln(2K\rho)}}{\rho^{\frac{5}{2}}}, \quad (106)$$

yielding, by comparison with (105),

$$f(\alpha) = \sum_n \left(\sum_m a_{n,m} \right) \Omega_n(\alpha). \quad (107)$$

In Ref. 90,91, several kinematic situations were studied and overall excellent agreement was found between the numerical hyperspherical expansion $\Psi^{NUM}(\rho, \alpha)$ and the analytical solution. An example is provided in Figure 7.7 for a fixed value $\alpha = \pi/4$. We show the comparison in two regions, close to the origin (left) and at very large hyperradii (right).

All hyperradial basis elements not only diagonalize the kinetic energy and the interaction, but also possess the same appropriate asymptotic behavior; thus, they only need to expand the solution in the interaction region. These properties strongly accelerate the expansion convergence rate for the scattering wave function, and allow for a straightforward extraction of the transition

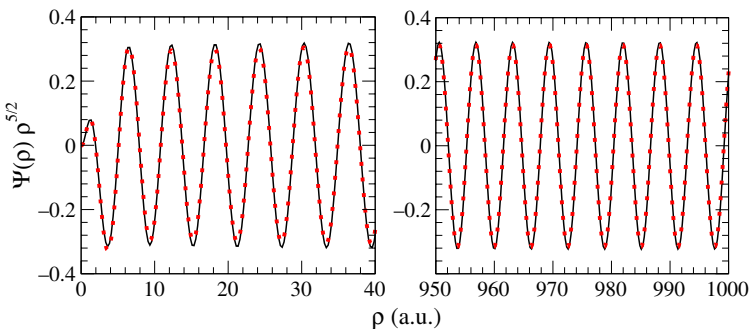


Figure 7.7 Real part of the numerical (full line) scattering solution $\Psi^{NUM}(\rho, \alpha)\rho^{5/2}$ given by Eq. (101) as a function of ρ along the cut $\alpha = \pi/4$, for $K = 1$ a.u. (i.e., the energy $E = 0.5$ a.u.), the parameters of the source are taken to be $a = 2$ and $t = 0$, and the interaction charge as $\mathcal{C} = -1$. The solid dots correspond to the real part of the analytical solution $\Psi^+(\rho, \alpha)\rho^{5/2}$. For color version of this figure, the reader is referred to the online version of this chapter.

amplitude. Excellent agreement with the analytical results is found with only very few expansion terms. The numerical results shown in [Figure 7.7](#) were obtained with only 8 hyperangular n - and 15 hyperradial m -terms.

The model problem allowed the authors^{90,91} to explore how the scattering wave function is modified in behavior for different hyperradial domains, and how far one should go to extract the transition amplitude from the wave function itself. It was found that the required hyperradial distances are very large, especially for low energies. With the GSF hyperspherical method, one can reach the truly outgoing asymptotic region, where no other numerical method (besides the propagations performed by Malegat et al.⁹⁶) can handle the calculations.

5.3 S-wave model of (e, 2e) processes on hydrogen

In this section, we review our results for the ionization of hydrogen by electron impact. To avoid all the difficulties introduced by the angular dependence of the wave functions and trying to clarify the crucial numerical and physical issues, we consider here the TP model:

$$\left[-\frac{1}{2r_1^2} \frac{\partial}{\partial r_1} \left(r_1^2 \frac{\partial}{\partial r_1} \right) - \frac{1}{2r_2^2} \frac{\partial}{\partial r_2} \left(r_2^2 \frac{\partial}{\partial r_2} \right) - \frac{Z}{r_1} - \frac{Z}{r_2} + \frac{1}{r_{>}} - E_a \right] \Psi_{sc}^+(r_1, r_2) = - \left[\left(\frac{1}{r_{>}} - \frac{1}{r_2} \right) \Psi_i(r_1, r_2) + (-1)^S (1 \leftrightarrow 2) \right]. \quad (108)$$

This is the standard test for any numerical method to be implemented for three-body ionization calculations, as it presents the difficulties associated to non-separability and to the long-range of the Coulomb potentials. As described in [Section 4.4](#), to solve [Eq. \(108\)](#), one may use a *CI* expansion [\(54\)](#) with a linear combination of properly symmetrized products of two-body outgoing Sturmian functions $S_{n_1 l_1}^+(r_1) S_{n_2 l_2}^+(r_2)$. In [Ref. 97](#), for each coordinate, a short-range generating potential, i.e., $\mathcal{V}(r_i) \rightarrow 0$ for $r_i > r_c$, was taken. On the other hand, choosing the auxiliary potential $\mathcal{U}(r_i)$, with a Coulomb tail, $-Z_i/r_i$ for $r_i > r_c$, provides an asymptotic behavior of the basis functions associated with an outgoing wave of energy E_i , distorted by the charge Z_i . The best way of defining the asymptotic behavior in each coordinate r_i corresponds to $E_i = E$ and $Z_i = Z - 1$. It actually corresponds to an appropriate description for the Ω_α region: one particle is at finite distance with close-to-zero or negative energy and sees the full

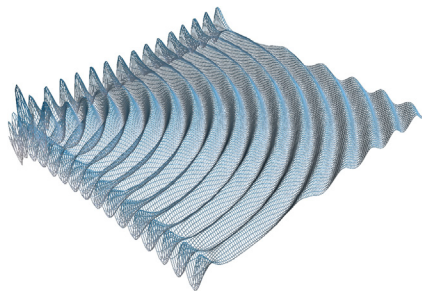


Figure 7.8 Schematic view of the real part of the scattering wave function evaluated with the Sturmian expansion. For color version of this figure, the reader is referred to the online version of this chapter.

nuclear charge Z while the other is at infinite distances carrying most of the system's energy but sees a screened charge Z_i . Since this screened value does not correspond to the atomic value at short distances, in order to have a more consistent picture, we define the potential $\mathcal{U}_i(r_i)$ by parts, i.e., $\mathcal{U}_i(r_i) = -Z/r_i$ for the inner region ($r < r_c$), and $\mathcal{U}_i(r_i) = -(Z - 1)/r_i$ for the outer region ($r > r_c$) (no major differences were observed between the results obtained with smooth or sharp charge transitions). The choice of the outer charge has a considerable effect in yielding a *CI* expansion convergence toward the correct asymptotic behavior and, at the same time, a smooth inner solution. On the other hand, the inner charge is not so important since in the inner region the expansion has to deal with the potentials not removed by the basis elements; by choosing $Z_i = Z$ in the inner region, though, the Sturmian functions diagonalize not only the kinetic energy but also the electron–nucleus potentials Z/r_i .

The typical form of a two–electron double continuum wave function obtained after solving Eq. (108) is shown in Figure 7.8 as a function of r_1 and r_2 . As expected from Eq. (56) an hyperspherical wave front can be clearly identified in a wide domain which includes the ionization region where $r_1 = r_2$ are both large. As we already explained in Section 4.1, the scattering wave function contains all channels at the same time and they are all coupled. On the borders of the figure, close to the axis $r_i = 0$, a different type of structure can be noticed and corresponds to the presence of excitation channels.

Once the wave function is obtained, various techniques can be applied to extract the cross-sections.

Before describing the SDCS results, we would like to add some comments on the convergence properties of the different approaches presented in the literature. As we have already mentioned, most of the computational

methods are based on the transformation of the Schrödinger equation into a linear system of equations. Its size is related to the number of basis elements employed. Computational limitation arises of course due to the limited size of the computer clusters. To reach convergence in a given spatial domain, a minimum number n_{min} of basis elements is required. This number depends on the kind of problem and efficiency of the basis employed. In Ref. 97 a detailed comparative study of the convergence rate of the GSF method in comparison with finite element method (FEM) was performed. The former was shown to perform better (faster and more stable). In order to compare the efficiency of the Sturmian expansion with respect to other techniques, we compared their density of basis elements d , a quantity defined as the number of total basis elements divided by the two-dimensional expanded area. First we can mention the work of Bartlett⁹⁸ who used the so-called propagating ECS (PECS) (designed to increase the numerical efficiency of the ECS), with a discrete variable representation with different grid regions. Results in a square domain of $R_0 = 220$ a.u. divided in $\simeq 625$ intervals were presented, yielding a density $d_{PECS} \simeq 626^2/220^2 \simeq 8.1$. Time-dependent calculation was performed by Pindzola and Robicheaux¹⁰⁰ using grid points characterized by $\Delta r = 0.2$ a.u. and domains of size $R_0 = 100$ a.u. to $R_0 = 500$ a.u. in steps of 100 a.u.. The best result for the TP model obtained with that method

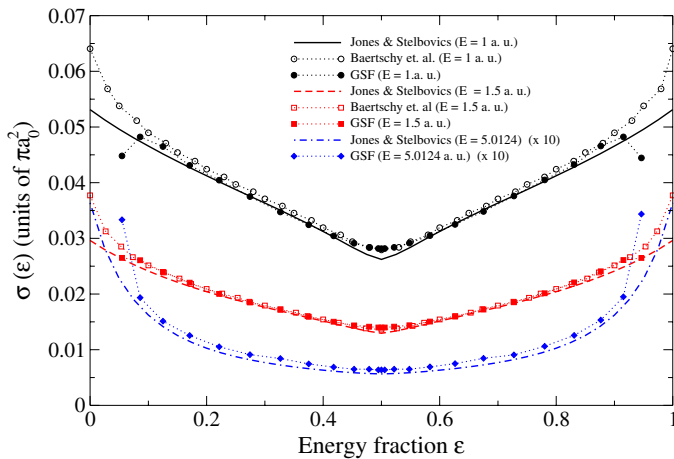


Figure 7.9 SDCS for different impact energies calculated with the GSF. The curves are constructed by evaluating the wave function flux at different hyperradius and then extrapolating the results to infinity. Also shown are the benchmark results of Jones and Stelbovics¹⁰⁰ and Baertschy and co-workers.¹⁰¹ For color version of this figure, the reader is referred to the online version of this chapter.

required a box of $R_0 = 500$ a.u., resulting into a density $d_{TD} = 25$. With the GSF expansion, converged SDCS were extracted from the wave function evaluated in a spatial domain with $r_c = 130$ a.u., and calculated with $N_s = 175$ basis functions per coordinate.⁹⁷ The resulting density $d_{GSF} = 0.9112$ illustrates the GSF method high efficiency.

As shown in [Section 4.3](#), ionization amplitudes can be extracted from the scattering wave function (see [Eq. \(56\)](#)). The corresponding SDCS, calculated with the GSF method, are shown in [Figure 7.9](#) for three different impact energies. They are evaluated at different and finite values of hyper-radius ρ and then extrapolated to $\rho \rightarrow \infty$.⁹⁷ For comparison, benchmark calculations of Jones and Stelbovics^{100,101} are also presented. All GSF results were performed with 150 Sturmian functions per coordinate and in a domain of 130 a.u..

Near the region $\alpha = 0$ and $\alpha = \pi/2$, the influence of the excitation channel appears, leading to differences in the SDCSs as the latter are obtained from the wave function itself. We are currently developing a technique to separate the individual channels contributions of the scattering wave function to be able to define appropriately such SDCS.

5.4 S-wave model of ($e, 3e$) processes on helium

Kinematically complete ($e, 3e$) experiments, in which the three outgoing particles are detected in coincidence, provide the most detailed information of electron impact double ionization of atoms.⁸² Absolute fivefold differential cross-sections for helium have been measured by the Orsay group^{12,83} in kinematic conditions such that the first Born approximation should be suitable. In spite of this, no theoretical study has yet managed to describe satisfactorily all the data. What is more confusing and difficult to explain, is that several *ab initio* methods provide different answers both in cross-section shapes and magnitudes (see a review in [Ref. 102](#)). From a theoretical point of view, the description of an ($e, 3e$) process on helium requires the solution of a pure four-body Coulomb problem. However, as discussed in [Section 4](#), reduction to a three-body problem can be performed in the case of high-energy projectiles as those used in the Orsay experiments.

In view of this unsatisfactory situation, the authors of [Ref. 80](#) looked for a simplified problem for which agreement between theoretical methods could possibly be found. They considered an S-wave ($e, 3e$) model with energy and geometry conditions used by the experimental Orsay group. The corresponding three-body model differs from that investigated in

Refs. 103,104, suitable for low-energy incident electrons, where the full four-body problem was considered.

Instead of considering the solution for the full first-order equation (72), they considered the following S -wave model⁸⁰

$$\left[-\frac{1}{2r_1^2} \frac{\partial}{\partial r_1} \left(r_1^2 \frac{\partial}{\partial r_1} \right) - \frac{1}{2r_2^2} \frac{\partial}{\partial r_2} \left(r_2^2 \frac{\partial}{\partial r_2} \right) - \frac{Z}{r_1} - \frac{Z}{r_2} + \frac{1}{r_{>}} - E_a \right] \Phi_{sc}^{(1)+}(r_1, r_2) = \mathcal{F}(r_1, r_2), \quad (109)$$

where

$$\mathcal{F}(r_1, r_2) = -\frac{1}{(2\pi)^3} \frac{4\pi}{q^2} [-Z + j_0(qr_1) + j_0(qr_2)] \Phi^{(0)}(r_1, r_2), \quad (110)$$

where $j_0(x)$ represents the spherical Bessel function of zeroth order, $\mathbf{q} = \mathbf{k}_i - \mathbf{k}_f$ is the momentum transfer, and $\Phi^{(0)}(r_1, r_2)$ is the ground-state solution of the S -wave helium equation Eq. (109) with the RHS set to zero. Moreover, since the idea was to provide benchmark values, all unnecessary ingredients were simplified and a simple ground state was taken: the product of screened exponentials $\Phi^{(0)}(r_1, r_2) = (Z_e^3/\pi) e^{-Z_e(r_1+r_2)}$ with $Z_e = Z - 5/16$.

The model equation (109) was numerically investigated with both Sturmian approaches described in Section 4. For the spherical coordinates approach, the numerical technique is essentially the one used above for the electron–Hydrogen problem and does not need to be repeated. For the hyperspherical approach, expansion (55) was used with the hyperradial Sturmian functions $S_{mn}^+(\rho)$ satisfying equation (87). The generating potential was taken to be of short-range (vanishing faster than ρ^{-1} as $\rho \rightarrow \infty$), and the auxiliary potential as a Coulomb potential with charge Z , thus imposing to the hyper-radial basis functions the desired asymptotic outgoing boundary condition (100) (with $\eta = \mu Z/K = \mu Z/\sqrt{2\mu E}$). Upon replacing either spherical (54) or hyperspherical (55) expansions into the scattering equation (109), and projecting onto the basis elements, one obtains a linear system

$$[\mathbf{H} - (E - \tilde{E})\mathbf{O}]\mathbf{a} = \mathbf{F}, \quad (111)$$

where \mathbf{H} and \mathbf{O} are the matrix representation of the Hamiltonian and overlap, and \mathbf{F} represents the RHS projected onto the basis set; \mathbf{a} is the vector of coefficients that builds the solution. For the spherical expansion $\tilde{E} = E_1 + E_2$; as the best choice of the Sturmian parameters is

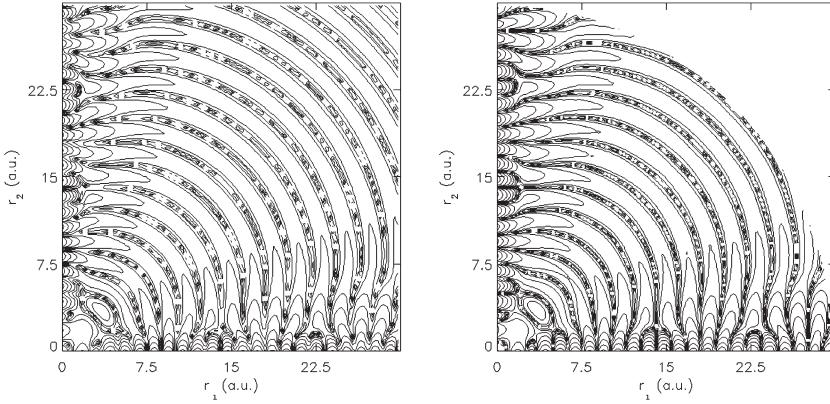


Figure 7.10 Left: Real part of the scattering wave function $\Phi_{sc}^{(1)+}(r_1, r_2) \times \rho^{5/2}$ as a function of the ejected electrons' radial coordinates r_1 and r_2 , for $E_a = 0.791$ a.u. and $q = 0.24$ a.u. Right: real part of $\Phi_{sc}^{(1)+}(\rho, \alpha) \times \rho^{5/2}$.

$E_1 = E_2 = E$, the overlap matrix elements have to be calculated. In the case of the hyperspherical expansion, $\tilde{E} = E$, so that no overlap matrix elements are required.

The (singlet, $S = 0$) solution $\Phi_{sc}^{(1)+}$ of Eq. (109) has been calculated with the two Sturmian expansions for several kinematical situations.⁸⁰ One of them is for a momentum transfer $q = 0.24$ a.u. which corresponds to the initial and final projectile energies of, respectively, $E_i = 5599$ eV and $E_f = 5500$ eV, and a deflection of 0.45° , used in the ($e, 3e$) Orsay experiment.⁸³ These values, together with the exact ground-state energy of the bound initial state, define the energy of the final three-body subsystem (1,2) equal to $\simeq 20$ eV. For an equal energy sharing situation, this corresponds to 10 eV per electron, as in the experiments.⁸³

The real part of the scattering solution, actually $\Phi_{sc}^{(1)+} \times \rho^{5/2}$, is shown as a function of r_1 and r_2 in the contour plots presented in Figure 7.10. The factor $\rho^{5/2}$ was chosen in order to keep the amplitude of the ionization (the hyperspherical outgoing wave) uniform as $\rho \rightarrow \infty$; it has to be noted that this factor increases the amplitude of single ionization channels (the peaks close the axis $r_1 = 0$ or $r_2 = 0$, i.e., the Ω_α regions) by the factor $\rho^{1/2}$. The result of the spherical expansion is shown in the left panel.

In the domain $r_1, r_2 > 5$ a.u., in which the driven term vanishes, the equation has the corresponding homogeneous equation solution. The basis functions for r_i values larger than r_c are simply products of outgoing

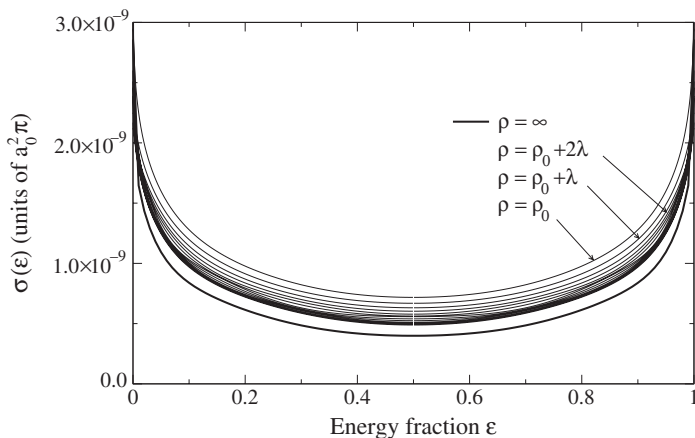
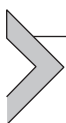


Figure 7.11 Single differential cross-section for the S -wave model ($e, 3e$) process for $q = 0.24$ a.u. The equal energy fraction value corresponds to ionized electron energies equal to 15 eV. SDCS evaluated with the flux formula for different values of $\rho_n = \rho_0 + n\lambda$ ($\lambda = \frac{2\pi}{\sqrt{2E}}$, $\rho_0 = 2\lambda$) are shown. The bottom solid line represents the $\rho \rightarrow \infty$ extrapolated result.

waves in spherical coordinates. However, as the figure shows, in the inner region they manage to generate the appropriate solution with a hyperspherical outgoing front, which is also observed in the electron–Hydrogen TP model. For comparison, the result obtained with the hyperspherical expansion is shown in the right panel; in this case the hyperspherical wave front is naturally generated by the basis. Thus, two completely independent codes and methods are leading to the same solution and the exact solution is obtained by enforcing outgoing type flux conditions on the basis set.

In Ref. 80, the main aim was to provide $e^- - \text{He}$ double ionization benchmark data within the above S -wave model. The transition amplitude for the double ionization process can be extracted from evaluating $|\Phi_{sc}^{(1)+}(\rho, \alpha) \rho^{5/2}|^2$ at large values of ρ . This technique is equivalent to taking the S -wave component of the transition amplitude defined by the integral (74); besides, it provides a verification of the scattering wave function's accuracy. From the transition amplitude one obtains a SDCS, noted $\sigma(q, \alpha)$, which should be independent of the hyperradial coordinate; effectively, one evaluates numerically σ_ρ at different values of ρ and then extrapolates the result to infinite distances with a form $\sigma \simeq \sigma_\rho + O[\rho^{-1}]$.⁹⁵ For a given q value, $\sigma(q, \alpha)$ is a singly differential cross-section which—through α (with $k_1 = K \cos \alpha$ and $k_2 = K \sin \alpha$)—describes how the energy is shared between the two ejected electrons. Such SDCS for S -wave double ionization of the

S-wave helium model have been presented as benchmark values in Ref. 80. A further example is provided by Figure 7.11, for two ejected electrons sharing 30 eV (the projectile's energy is 5600 eV and the momentum transfer $q = 0.24$ a.u. as in the Orsay experiment). This SDCS was obtained with the spherical GSF and confirmed by the hyperspherical Sturmian approach. No comparison with other calculations could be presented since they are the first calculations of the process at the considered projectile energy. The study aimed to stimulate other numerical methods: if agreement can be found for the present model, one would then attribute the existing differences for the real ($e, 3e$) process¹⁰² to $L \neq 0$ and/or convergence issues.



6. SUMMARY AND PERSPECTIVES

In this paper we presented a review of some applications of the Generalized Sturmian Method. We want to stress once again that remarkable work has been done by other researchers but mostly using Coulomb Sturmian functions, and not generalized ones. The work of Macek and Ovchinnikov,^{29–34} and Rawistcher^{24–27} on Generalized Sturmian functions had a profound influence on our research. The work of Piraux,⁹ Avery,^{17,18} Aquilanti,^{21,22,105} Goscinski,¹⁰⁶ Manakov,¹⁰⁷ Shakeshaft,¹⁰⁸ Rotenberg,¹⁰⁹ Szymkowski,^{110,111} and Maquet,^{112,113} among others, have also been of great importance for the development of most of our investigations.

In Section 2 we gave a short description of the Generalized Sturmian Function theory and how this is applied in two-body problems. We gave also a numerical example where the two-body Coulomb problem is reformulated within the short-range scattering theory. The application of the method to three-body bound states is discussed in Section 3. We started by reviewing the results for the He and H^- systems. We showed that the convergence of the energies can be substantially improved when the GSF are used instead of CSE. The best energies obtained with uncorrelated basis have been produced using GSE.⁴² We proved that optimizing the asymptotic property of the basis functions, the appropriate behavior can be generated in the three-body wave functions. This was shown for He-like atoms, for the H_2^+ molecule, as well as some exotic systems, but even more clearly for He doubly excited states. In this case imposing outgoing-type behavior to the GSF we obtained not only the real part of the energies but also their corresponding lifetimes. The method is robust enough to allow the inclusion of general auxiliary potentials in the Sturmian equation. This

facilitates, for example, treatment of confined systems. We exemplified its robustness performing energy calculations of He atoms confined in a model cage representing a C_{60} fullerene, and in an impenetrable cage. All these calculations can be performed with high accuracy; the latter can be increased as much as necessary to recognize the avoided crossing structure appearing in both systems.

The description of scattering problems is based on the solution of a driven equation. The wave function of the problem is separated into a prepared initial state and a scattering state. All the physics about the collision is condensed into the scattering part of the wave function, which satisfies the driven equation. In [Section 2](#) we showed how to apply the GSF method to two-body problems. As an example of the application we defined a distorted wave approach to enable inclusion of Coulomb potentials into the standard scattering theory. In [Section 4](#), we first derived the driven equations for the single ionization of hydrogen atom by electron impact and for the double ionization of He by high-energy electron impact. Both problems lead to the same type of driven equation. Two Sturmian approaches were discussed as tools to solve it. One is based on the product of GSF in $\mathbf{r}_1, \mathbf{r}_2$ coordinates. In an alternative approach, the radial coordinates r_1, r_2 are replaced by ρ and α , the hyperspherical radius and angle. In both cases the scattering wave function is forced to have purely outgoing behavior at large values of ρ . This condition is built in the spherical approach, while it is natural in the case of the hyperspherical approach, for the cases under scrutiny.

In [Section 5](#), we presented the application of the GSF method to the solution of three benchmark model problems. All of them correspond to S -wave models. The first one possesses analytical solution in hyperspherical coordinates. We used our hyperspherical GSF recipe to solve the problem and found perfect agreement for all the cases considered. Secondly, we evaluated the electron-impact ionization of Hydrogen within the S -wave model. In this case we compared our results with those provided by other methods. As a third example, we considered an S -wave model for the double ionization of He by high-energy electron impact. As the model was introduced only very recently, no other calculations are available for comparison. However, we checked our results by computing the solution of the problem using the spherical and the hyperspherical approaches: agreement between both methods is remarkable. In all the cases it can be verified that the expected hyperspherical wave front is effectively built by the GSF method. The corresponding cross-sections can be extracted directly from the asymptotic limit of the wave function.

Results for the full ($e, 2e$) and ($e, 3e$) processes as well as for double photoionization of atoms are presently being obtained and soon will be published elsewhere.

In the present review, we presented GSF in spherical and hyperspherical coordinates. However, as mentioned in Ref. 35 parabolic coordinates could be very useful to deal with many interesting problems where Coulomb potentials appear. Indeed, very important studies have been performed using these coordinates. The group of Aquilanti and collaborators has done remarkable progress on the treatment of bound states using parabolic CSF.^{114,115} Ojha,¹¹⁶ Burgdörfer,¹¹⁷ Piraux,^{118,119} and Zaytsev,^{120–124} among others, have considered using CSF in parabolic coordinates for the treatment of two- and three-body problems involving in many cases ionization. The study and implementation of GSF and quasi-Sturmian functions in parabolic¹²³ and spherical coordinates¹²⁵ is the object of the actual investigations which are being performed in collaboration with Zaytsev. These investigations extend and formalize the studies initiated in the 1990s by Garibotti's^{78,126,75,77} and Miraglia's^{76,127} groups.

The application of GSF to the study many-electron atoms and molecular systems is the purpose of our current research.

ACKNOWLEDGMENTS

The authors kindly acknowledge the enlightening discussions with Prof. Rawitscher and his careful reading of this paper. The authors also thank the careful revisions performed by Profs. Piraux, Aquilanti, and Avery. The authors very much acknowledge the invaluable support given by different agencies and universities along these years: the Agencia Nacional de Promoción Científica y Tecnológica (ANPCyT) PICT 0934/08 and PICT 04/20548); the Consejo Nacional de Investigaciones Científicas y Técnicas (CONICET), PIP 200901/552 and PIP 5595. The authors also acknowledge support from the Universidad de Buenos Aires (UBACyT), Universidad Nacional de Cuyo (06/C279, 06/C229, 06/C348 grants), Universidad Nacional del Sur (PGI), and Université de Lorraine, and the French-Argentinian program ECOS-Sud A10E01.

REFERENCES

1. Drake, G.W.F. *Springer Handbook of Atomic, Molecular, and Optical Physics*; Springer: New York, 2005.

2. Kresse, G.; Hafner, J. Ab Initio Molecular Dynamics for Liquid Metals. *Phys. Rev. B* **1993**, *47*, 558. Kresse, G.; Hafner, J. Ab Initio Molecular-Dynamics Simulation of the Liquid-Metamorphous-Semiconductor Transition in Germanium. *Phys. Rev. B* **1994**, *49*, 14251.
3. Frisch, M. J. et al. *Gaussian 09, Revision A.1*, Gaussian Inc., Wallingford, CT, 2009.
4. Avery, J. *Hyperspherical Harmonics and Generalized Sturmians*; Kluwer Academic Publishers: Dordrecht, The Netherlands, 2000.
5. Avery, J.; Avery, J. *Generalized Sturmians and Atomic Spectra*; World Scientific: Singapore, 2006.
6. Avery, J.; Avery, J. Coulomb Sturmians as a Basis for Molecular Calculations. *Mol. Phys.* **2012**, *110*, 10.
7. Newton, R. G. *Scattering Theory of Waves and Particles*; Dover Publications Inc.: New York, 2002.
8. Kadyrov, A. S.; Mukhamedzhanov, A. M.; Stelbovics, A. T.; Bray, I.; Pirlepesov, F. Asymptotic Behavior of the Coulomb Three-Body Scattered Wave. *Phys. Rev. A* **2003**, *68*, 022703.
9. Fomouuo, E.; Kamta, G. L.; Edah, G.; Piraux, B. Theory of Multiphoton Single and Double Ionization of Two-Electron Atomic Systems Driven by Short-Wavelength Electric Fields: An Ab Initio Treatment. *Phys. Rev. A* **2006**, *74*, 063409.
10. Knyr, V. A.; Nasyrov, V. V.; Popov, Yu. V.; Ya Stotland, L. Application of the J-Matrix Method to Problems of Single Ionization of Atoms by Fast Electrons. *J. Exp. Theor. Phys.* **1996**, *82*, 190.
11. Silenou Mengoue, M.; Kwato Njock, M. G.; Piraux, B.; Popov, Yu. V.; Zaytsev, S. A. Electron-Impact Double Ionization of He by Applying the Jacobi Matrix Approach to the Faddeev-Merkuriev Equations. *Phys. Rev. A* **2011**, *83*, 052708.
12. Kheifets, A.; Bray, I.; Lahmam-Bennani, A.; Duguet, A.; Taouil, I. A Comparative Experimental and Theoretical Investigation of the Electron-Impact Double Ionization of He in the keV Regime. *J. Phys. B* **1999**, *32*, 5047.
13. McCurdy, C. W.; Horner, D. A.; Rescigno, T. N.; Martín, F. Theoretical Treatment of Double Photoionization of Helium Using a B-Spline Implementation of Exterior Complex Scaling. *Phys. Rev. A* **2004**, *69*, 032707.
14. Gasaneo, G.; Ancarani, L. U.; Mitnik, D. M. On the Applicability of the Exterior Complex Scaling Method for Scattering Problems Including Coulombic Potentials. *Eur. Phys. J. D* **2012**, *66*, 91.
15. Rescigno, T. N.; Baertschy, M.; Isaacs, W. A.; McCurdy, C. W. Collisional Breakup in a Quantum System of Three Charged Particles. *Science* **1999**, *286*, 2474.
16. Stelbovics, A. T. Calculation of Ionization within the Close-Coupling Formalism. *Phys. Rev. Lett.* **1999**, *83*, 1570.
17. Avery, J.; Avery, J. Generalized Sturmian Solutions for Many-Particle Schrödinger Equations. *J. Phys. Chem. A* **2004**, *108*, 8848–8851.
18. Avery, J.; Avery, J. The Generalized Sturmian Method for Calculating Spectra of Atoms and Ions. *J. Math. Chem.* **2003**, *33*, 145.
19. Avery, J.; Shim, R. Molecular Sturmians. Part 1. *Int. J. Quantum Chem.* **2001**, *83*, 1–10.
20. Aquilanti, V.; Cavalli, S.; Coletti, C.; Grossi, G. Alternative Sturmian Bases and Momentum Space Orbitals: An Application to the Hydrogen Molecular Ion. *Chem. Phys.* **1996**, *209*, 405.
21. Aquilanti, V.; Cavalli, S.; De Fazio, D. J. Hyperquantization Algorithm. I: Theory for Triatomic Systems. *Chem. Phys.* **1998**, *109*, 3792.
22. Aquilanti, V.; Cavalli, S.; De Fazio, D.; Volpi, A.; Aguilar, A.; Gimenez, X.; Lucas, J. M. Hyperquantization Algorithm. II: Implementation for the $F1\ H_2$ Reaction Dynamics Including Open-Shell and Spin-Orbit Interactions. *J. Chem. Phys.* **1998**, *109*, 721.

23. Aquilanti, V.; Cavalli, S.; Coletti, C.; Di Domenico, D.; Grossi, G. Hyperspherical Harmonics as Sturmian Orbitals in Momentum Space: A Systematic Approach to the Few-Body Coulomb Problem. *Int. Rev. Phys. Chem.* **2001**, *20*, 673.
24. Rawitscher, G. Positive Energy Weinberg States for the Solution of Scattering Problems. *Phys. Rev. C* **1982**, *25*, 2196.
25. Rawitscher, G. Separable Representation of the Two-Body Reid Soft Core T Operator in Terms of Positive Energy Weinberg States. *Phys. Rev. C* **1989**, *39*, 440.
26. Rawitscher, G. In *Topics in Theoretical Physics*, Aguilera-Navarro, V. C., Galetti, D., Pimentel, B. M., Tomio, L. Instituto de Física Teórica, **1995**, pp 255.
27. Rawitscher, G. Iterative Solution of Integral Equations on a Basis of Positive Energy Sturmian Functions. *Phys. Rev. E* **2012**, *85*, 026701.
28. Rawitscher, G. Iterative Evaluation of the Effect of Long-Range Potentials on the Solution of the Schrödinger equation. *Phys. Rev. A* **2013**, *87*, 032708.
29. Yu, S. Electron-Energy and Angular-Distribution Theory for Low-Energy Ion-Atom Collisions. *Phys. Rev. Lett.* **1995**, *75*, 2474.
30. Macek, J. H.; Yu Ovchinnikov, S. Hyperspherical Theory of Three-Particle Fragmentation and Wannier Threshold Law. *Phys. Rev. A* **1996**, *54*, 544.
31. Yu Ovchinnikov, S.; Macek, J. H. Positive Energy Sturmian States for Two-Coulomb-Center Problems. *Phys. Rev. A* **1997**, *55*, 3605.
32. Gasaneo, G.; Macek, J. H. Hyperspherical Adiabatic Eigenvalues for Zero-Range Potentials. *J. Phys. B* **2002**, *35*, 2239.
33. Macek, J. H.; Yu Ovchinnikov, S.; Gasaneo, G. Solution for Boson-Diboson Elastic Scattering at Zero Energy in the Shape-Independent Model. *Phys. Rev. A* **2005**, *72*, 032709.
34. Macek, J. H.; Yu Ovchinnikov, S.; Gasaneo, G. Exact Solution for Three Particles Interacting via Zero-Range Potentials. *Phys. Rev. A* **2006**, *73*, 032704.
35. Gasaneo, G.; Colavecchia, F. D. Two-Body Coulomb Wavefunctions as Kernel for Alternative Integral Transformations. *J. Phys. A* **2003**, *36*, 8443.
36. Frapiccini, A. L.; Gasaneo, G.; Colavecchia, F. D.; Mitnik, D. Sturmian Functions in a L^2 Basis: Critical Nuclear Charge for n-Electron Atoms. *J. Electron. Spectrosc. Relat. Phenom.* **2007**, *161*, 199–203.
37. Frapiccini, A. L.; Gonzalez, V. Y.; Randazzo, J. M.; Colavecchia, F. D.; Gasaneo, G. L^2 Discretization of Sturmian Wave Functions for Coulomb-like Potentials. *Int. J. Quant. Chem.* **2007**, *107*, 832–844.
38. Randazzo, J. M.; Frapiccini, A. L.; Colavecchia, F. D.; Gasaneo, G. *Phys. Rev. A* **2009**, *79*, 022507; Randazzo, J. M. Métodos ab initio para el problema de tres cuerpos con interacciones Coulombianas, Ph.D. thesis, Instituto Balseiro, Universidad Nacional de Cuyo, Argentina, 2009.
39. Randazzo, J. M.; Frapiccini, A. L.; Colavecchia, F. D.; Gasaneo, G. Discrete Sets of Many-Body Sturmians. *Int. J. Quantum Chem.* **2009**, *109*, 125.
40. Randazzo, J. M.; Gasaneo, G.; Colavecchia, F. D. A General Method to Obtain Sturmian Functions for Scattering and Bound State Problems. *Int. J. Quantum Chem.* **2010**, *110*, 963–974.
41. Frapiccini, A. L.; Randazzo, J. M.; Gasaneo, G.; Colavecchia, F. D. *J. Phys. B* **2010**, *43*, 101001; Frapiccini, A. L. Descripción de la dinámica de electrones en interacción con átomos, Ph.D. thesis, Instituto Balseiro, Universidad Nacional de Cuyo, Argentina, 2010.
42. Randazzo, J. M.; Ancarani, L. U.; Gasaneo, G.; Frapiccini, A. L.; Colavecchia, F. D. Generating Optimal Sturmian Basis Functions for Atomic Problems. *Phys. Rev. A* **2010**, *81*, 042520.
43. Mitnik, D. M.; Colavecchia, F. D.; Gasaneo, G.; Randazzo, J. M. Computational Methods for Generalized Sturmians Basis. *Comput. Phys. Commun.* **2011**, *182*, 1145.
44. Ambrosio, M. J.; Del Punta, J. A.; Rodriguez, K. V.; Gasaneo, G.; Ancarani, L. U. Mathematical Properties of Generalized Sturmian Functions. *J. Phys. A* **2012**, *45*, 015201.

45. Luk, F. T.; Qiao, S. A Fast Eigenvalue Algorithm for Hankel Matrices. *Linear Algebra Appl.* **2000**, *316*, 171.
46. Broad, J. T. Calculation of Two-Photon Processes in Hydrogen with an L^2 Basis. *Phys. Rev. A* **1985**, *31*, 1494.
47. de Boor, C. *A Practical Guide to Splines*; Springer: New York, 1978.
48. Shull, H.; Löwdin, P. O. Superposition of Configurations and Natural Spin Orbitals. Applications to the He Problem. *J. Chem. Phys.* **1959**, *30*, 617.
49. Bromley, M. W. J.; Mitroy, J. Convergence of the Partial Wave Expansion of the He Ground State. *Int. J. Quantum Chem.* **2007**, *107*, 1150.
50. Goldman, S. P. Uncoupling Correlated Calculations in Atomic Physics: Very High Accuracy and Ease. *Phys. Rev. A* **1998**, *57*, R677.
51. Freund, D. E.; Huxtable, B. D.; Morgan, J. D. Variational Calculations on the Helium Isoelectronic Sequence. *Phys. Rev. A* **1984**, *29*, 980.
52. Frapiccini, A. L.; Randazzo, J. M.; Gasaneo, G.; Colavecchia, F. D. Sturmian Expansion of Two-Electron Atomic Systems: Singly and Doubly Excited States. *Phys. Rev. A* **2010**, *82* 042503
53. Eiglsperger, J.; Piraux, B.; Madronero, J. Spectral Representation of the Three-Body Coulomb Problem: Perspectives for Highly Doubly Excited States of Helium. *Phys. Rev. A* **2009**, *80*, 022511.
54. Eiglsperger, J.; Piraux, B.; Madronero, J. Spectral Representation of the Three-Body Coulomb Problem. I: Non-Autoionizing Doubly-Excited States of High Angular Momentum in Helium. *Phys. Rev. A* **2010**, *81*, 042527.
55. Eiglsperger, J.; Piraux, B.; Madronero, J. Spectral Representation of the Three-Body Coulomb Problem. II: Autoionizing Doubly-Excited States of Unnatural Parity in Helium. *Phys. Rev. A* **2010**, 042528.
56. Eiglsperger, J.; Schwetter, M.; Piraux, B.; Madroero, J. Spectral Data for Doubly Excited States of Helium with Non-Zero Total Angular Momentum. *At. Data Nuclear Data Tables* **2012**, *98*, 120–148.
57. Drake, G. W. F. Variational Eigenvalues for the Rydberg States of Helium: Comparison with Experiment and with Asymptotic Expansions. *Phys. Rev. Lett.* **1990**, *65*, 2769; Drake, G. W. F.; Yan, Z. C. Energies and Relativistic Corrections for the Rydberg States of Helium: Variational Results and Asymptotic Analysis. *Phys. Rev. A* **1992**, *46*, 2378.
58. Bürgers, A.; Wintgen, D.; Rost, J. M. Highly Doubly Excited S States of the Helium Atom. *J. Phys. B* **1995**, *28*, 3163.
59. Rodriguez, K. V. Bases Correlacionadas Aplicadas al Estudio de Sistemas de Tres Cuerpos Generales, Ph.D. Thesis, Departamento de Física, Universidad Nacional del Sur, Argentina, 2010.
60. Ancarani, L. U.; Rodriguez, K. V.; Gasaneo, G. Correlated $n^{1,3}$ S States for Coulomb Three-Body Systems. *Int. J. Quantum Chem.* **2011**, *111*, 4255.
61. Drake, G. W. F.; Grigorescu, M. Binding Energy of the Positronium Negative Ion: Relativistic and QED Energy Shifts. *J. Phys. B* **2005**, *38*, 3377.
62. Korobov, V. I. Coulomb Three-Body Bound-State Problem: Variational Calculations of Nonrelativistic Energies. *Phys. Rev. A* **2000**, *61*, 064503.
63. Mitnik, D. M.; Randazzo, J.; Gasaneo, G. Endohedrally Confined Helium: Study of Mirror Collapses. *Phys. Rev. A* **2008**, *78*, 062501.
64. Colavecchia, F. D.; Gasaneo, G.; Mitnik, D. Double Photoionization of Endohedrally Confined Atoms. *J. At. Mol. Opt. Phys.* **2011**, *2011*, 817034.
65. Xu, Y. B.; Tan, M. Q.; Becker, U. Oscillations in the Photoionization Cross Section of C_60 . *Phys. Rev. Lett.* **1996**, *76*, 3538.

66. Connerade, J. P.; Dolmatov, V. K.; Lakshmi, P. A.; Manson, S. T. Electron Structure of Endohedrally Confined Atoms: Atomic Hydrogen in an Attractive Shell. *J. Phys. B* **1999**, *32*, L239.
67. Banerjee, A.; Kamal, C.; Chowdhury, A. Calculation of Ground- and Excited-State Energies of Confined Helium Atom. *Phys. Lett. A* **2006**, *350*, 121.
68. Aquino, N.; Flores-Riveros, A.; Rivas-Silva, J. F. The Compressed Helium Atom Variationally Treated Via a Correlated Hylleraas Wave Function. *Phys. Lett. A* **2003**, *307*, 326.
69. Papp, P.; Plessas, W. Coulomb-Sturmian Separable Expansion Approach: Three-Body Faddeev Calculations for Coulomb-like Interactions. *Phys. Rev. C* **1996**, *54*, 50.
70. Papp, Z.; Darai, J.; Hu, C.-Y.; Hlousek, Z. T.; Koňya, Z. T.; Yakovlev, S. L. Resonant-State Solution of the Faddeev-Merkuriev Integral Equations for Three-Body Systems with Coulomb Potentials. *Phys. Rev. A* **2002**, *65*, 032725.
71. Joslin, C.; Goldman, S. Quantum Monte Carlo Studies of Two-Electron Atoms Constrained in Spherical Boxes. *J. Phys. B* **1992**, *25*, 1965.
72. Garibotti, C. R.; Miraglia, J. E. Ionization and Electron Capture to the Continuum in the H^+ -Hydrogen-Atom Collision. *Phys. Rev. A* **1980**, *21*, 572.
73. Brauner, M.; Briggs, J. S.; Klar, H. Triply-Differential Cross Sections for Ionisation of Hydrogen Atoms by Electrons and Positrons. *J. Phys. B* **1989**, *22*, 2265.
74. Alt, E. O.; Mukhamedzhanov, A. M. Asymptotic Solution of the Schrödinger Equation for Three Charged Particles. *Phys. Rev. A* **1993**, *47*, 2004.
75. Colavecchia, F. D.; Gasaneo, G.; Garibotti, C. R. Separable Wave Equation for Three Coulomb Interacting Particles. *Phys. Rev. A* **1998**, *57*, 1018.
76. Macri, P.; Miraglia, J. E.; Garibotti, C. R.; Colavecchia, F. D.; Gasaneo, G. Approximate Analytical Solution for Two Electrons in the Continuum. *Phys. Rev. A* **1997**, *55*, 3518.
77. Colavecchia, F. D.; Gasaneo, G.; Garibotti, C. R. Electron-Ion Correlation Effects in Ion-Atom Single Ionization. *J. Phys. B* **2000**, *33*, L467.
78. Gasaneo, G.; Colavecchia, F. D.; Garibotti, C. R.; Miraglia, J. E.; Macri, P. Correlated Continuum Wave Functions for Three Particles with Coulomb Interactions. *Phys. Rev. A* **1997**, *55*, 2809.
79. Gasaneo, G.; Ancarani, L. U. Use of Double-Bound Three-Body Coulomb Distorted-Wave-like Basis Sets for Two-Electron Wave Functions. *Phys. Rev. A* **2008**, *77*, 012705.
80. Gasaneo, G.; Mitnik, D. M.; Randazzo, J. M.; Ancarani, L. U.; Colavecchia, F. D. S-Model Calculations for High-Energy-Electron-Impact Double Ionization of Helium. *Phys. Rev. A* **2013**, *87*, 042707.
81. Joachain, C. J. *Quantum Collision Theory*, North-Holland Publishing Company, 1983.
82. Berakdar, J.; Lahmam-Bennani, A.; Dal Cappello, C. The Electron-Impact Double Ionization of Atoms: An Insight into the Four-Body Coulomb Scattering Dynamics. *Phys. Rep.* **2003**, *374*, 91.
83. Lahmam-Bennani, A., et al. Origin of Dips and Peaks in the Absolute Fully Resolved Cross Sections for the Electron-Impact Double Ionization of He. *Phys. Rev. A* **1999**, *59*, 3548.
84. Gasaneo, G.; Mitnik, D. M.; Frapiccini, A. L.; Colavecchia, F. D.; Randazzo, J. M. Theory of Hyperspherical Sturmians for Three-Body Reactions. *J. Phys. Chem. A* **2009**, *113*, 14573.
85. Colavecchia, F. D.; Mrugala, F.; Parker, G. A.; Pack, R. T. Accurate Quantum Calculations on Three-Body Collisions in Recombination and Collision-Induced Dissociation. II: The Smooth Variable Discretization Enhanced Renormalized Numerov Propagator. *J. Chem. Phys.* **2003**, *118*, 10387.
86. Gasaneo, G.; Ancarani, L. U. A Spectral Approach Based on Generalized Sturmian Functions for Two- and Three-Body Scattering Problems. *J. Phys. A* **2012**, *45*, 045304.

87. Abramowitz, M.; Stegun, I. A. *Handbook of Mathematical Functions*; Dover: New York, 1972.
88. Temkin, A. Nonadiabatic Theory of Electron-Hydrogen Scattering. *Phys. Rev.* **1962**, *126*, 130.
89. Poet, R. The Exact Solution for a Simplified Model of Electron Scattering by Hydrogen Atoms. *J. Phys. B* **1978**, *11*, 3081.
90. Ancarani, L. U.; Gasaneo, G.; Mitnik, D. M. An Analytically Solvable Three-Body Break-Up Model Problem in Hyperspherical Coordinates. *Eur. Phys. J. D* **2012**, *66*, 270/1-11.
91. Mitnik, D. M.; Gasaneo, G.; Ancarani, L. U. Use of Generalized Hyperspherical Sturmian Functions for a Three-Body Break-Up Model Problem. *J. Phys. B* **2013**, *46*, 015202.
92. Dongarra, J., et al. *Lapack User's Guide*; 3rd ed.; SIAM: Philadelphia, USA, 1999.
93. Ancarani, L. U.; Gasaneo, G. Two-Body Coulomb Problems with Sources for the J-Matrix Method. *J. At. Mol. Sci.* **2011**, *2*, 203.
94. Rudge, M. R. H. Theory of the Ionization of Atoms by Electron Impact. *Rev. Mod. Phys.* **1968**, *40*, 564.
95. Peterkop, R. K. *Theory of Ionization of Atoms by Electron Impact*; Colorado Associated University Press: Boulder, CO, 1977.
96. Malegat, L.; Selles, P.; Kazansky, A. K. Absolute Differential Cross Sections for Photo Double Ionization of Helium from the Ab Initio Hyperspherical R-Matrix Method with Semiclassical Outgoing Waves. *Phys. Rev. Lett.* **2000**, *85*, 4450.
97. Randazzo, J. M.; Buezas, F.; Frapiccini, A. L.; Colavecchia, F. D.; Gasaneo, G. Solving Three-Body-Breakup Problems with Outgoing-Flux Asymptotic Conditions. *Phys. Rev. A* **2011**, *84*, 052715.
98. Bartlett, P. L. A Complete Numerical Approach to Electronhydrogen Collisions. *J. Phys. B* **2006**, *39*, R379.
99. Pindzola, M. S.; Robicheaux, F. Differential Cross Sections in the Ejected Energy for an $L=0$ Model of the Electron-Impact Ionization of Hydrogen. *Phys. Rev. A* **1997**, *55*, 4617.
100. Jones, S.; Stelbovics, A. T. Efficient Solution of Three-Body Quantum Collision Problems: Application to the Temkin-Poet Model. *Phys. Rev. A* **2002**, *66*, 032717.
101. Baertschy, M.; Rescigno, T. N.; Isaacs, W. A.; McCurdy, C. W. Benchmark Single-Differential Ionization Cross Section Results for the s-Wave Model of Electron-Hydrogen Scattering. *Phys. Rev. A* **1999**, *60*, R13.
102. Ancarani, L. U.; Dal Cappello, C.; Gasaneo, G. Double Ionization of Two-Electron Systems. *J. Phys.: Conf. Ser.* **2010**, *212*, 012025.
103. Bartlett, P. L.; Stelbovics, A. T. Electron-Helium S-Wave Model Benchmark Calculations. I: Single Ionization and Single Excitation. *Phys. Rev. A* **2010**, *81*, 022715.
104. Bartlett, P. L.; Stelbovics, A. T. Electron-Helium S-Wave Model Benchmark Calculations. II: Double Ionization, Single Ionization with Excitation, and Double Excitation. *Phys. Rev. A* **2010**, *81*, 022716.
105. Aquilanti, V.; Cavalli, S.; Coletti, C. Hyperspherical Symmetry of Hydrogenic Orbitals and Recoupling Coefficients among Alternative Bases. *Phys. Rev. Lett.* **1998**, *80*, 3209.
106. Goscinski, O. *Preliminary Research Report No. 217*, Quantum Chemistry Group, Uppsala University, 1968.
107. Krylovetsky, A. A.; Manakov, N. L.; Marmo, S. I. Generalized Sturm Expansions of the Coulomb Green Function and Two-Photon Gordon Formulas. *J. Exp. Theor. Phys.* **2001**, *92*, 37.
108. Shakeshaft, R. Sturmian Expansion of Green Function and its Application to Multiphoton Ionization of Hydrogen. *Phys. Rev. A* **1986**, *34*, 244.

109. Rotenberg, M. Theory and Application of Sturmian Functions. *Adv. At. Mol. Phys.* **1970**, *6*, 233.
110. Szmytkowski, R. The Continuum Schrödinger-Coulomb and Dirac-Coulomb Sturmian Functions. *J. Phys. A* **1998**, *31*, 4963.
111. Szmytkowski, R. Remarks on Completeness of Many-Electron Sturmians. *J. Phys. A* **2000**, *33*, 4553.
112. Maquet, A. Use of the Coulomb Green's Function in Atomic Calculations. *Phys. Rev. A* **1977**, *15*, 1088.
113. Maquet, A.; Vénier, V.; Marian, T. A. The Coulomb Green Function and Multiphoton Calculations. *J. Phys. B* **1998**, *31*, 3743.
114. Aquilanti, V.; Cavalli, S.; Coletti, C. The d-Dimensional Hydrogen Atom: Hyperspherical Harmonics as Momentum Space Orbital and Alternative Sturmian Basis Sets. *Chem. Phys.* **1997**, *214*, 1.
115. Aquilanti, V.; Calagiana, A.; Cavalli, S. Hydrogenic Elliptic Orbitals, Coulomb Sturmian Sets, and Recoupling Coefficients Among Alternative Bases. *J. Quantum Chem.* **2003**, *92*, 99.
116. Ojha, P. C. The Jacobi-Matrix Method in Parabolic Coordinates: Expansion of Coulomb Functions in Parabolic Sturmians. *J. Math. Phys.* **1987**, *28*, 392.
117. Yoshida, S.; Reinhold, C. O.; Burgdorfer, J. Accurate Ionization Thresholds of Atoms Subject to Half-Cycle Pulses. *Phys. Rev. A* **1998**, *58*, 2229.
118. Bugacov, A.; Piraux, B.; Pont, M.; Shakeshaft, R. Asymmetry in Ionization of Oriented Rydberg States of Hydrogen by a Half-Cycle Pulse. *Phys. Rev. A* **1995**, *51*, 4877.
119. Bugacov, A.; Piraux, B.; Pont, M.; Shakeshaft, R. Ionization of Rydberg Hydrogen by a Half-Cycle Pulse. *Phys. Rev. A* **1995**, *51*, 1490.
120. Zaytsev, S. A. One- and two-Dimensional Coulomb Green Function Matrices in Parabolic Sturmians Basis. *J. Phys. A* **2008**, *41*, 265204.
121. Zaytsev, S. A. The Parabolic Sturmian-Function Basis Representation of the Six-Dimensional Coulomb Green Function. *J. Phys. A* **2009**, *42*, 015202.
122. Zaytsev, S. A. Representation of the Three-Body Coulomb Green's Function in Parabolic Coordinates: Paths of Integration. *J. Phys. A* **2010**, *43*, 385208.
123. Zaytsev, S. A.; Gasaneo, G. Solving a Three-Body Continuum Coulomb Problem with Quasi-Sturmian Functions. *J. At. Mol. Sci.* **2013**, *4*, 302–320.
124. Zaytsev, S. A.; Popov, Yu V.; Piraux, B. Parabolic Sturmians Approach to the Three-Body Continuum Coulomb Problem. *Phys. At. Nuclei* **2013**, *76*, 365.
125. Del Punta, J. A.; Ambrosio, M. J.; Gasaneo, G.; Zaytsev, S. A.; Ancarani, L. U. Non-Homogeneous Solutions of a Coulomb Schrödinger equation as basis set for scattering problems. *J. Phys. A*, **2013**.
126. Gasaneo, G.; Colavecchia, F. D.; Garibotti, C. R.; Miraglia, J. E.; Macri, P. Multivariable Hypergeometric Solutions for Three Charged Particles. *J. Phys. B* **1997**, *30*, L265.
127. Miraglia, J. E.; Bustamante, M. G.; Macri, P. A. Approximate Wave Functions for Two Electrons in the Continuum of a Coulomb Charge. *Phys. Rev. A* **1999**, *60*, 4532.